Development and Application of a Lubricant Composition Model to Study Effects of Oil Transport, Vaporization, Fuel Dilution, and Soot Contamination on Lubricant Rheology and Engine Friction

by

Grace Xiang Gu

B.S., Mechanical Engineering
University of Michigan, 2012

Submitted to the Department of Mechanical Engineering
in partial fulfillment of the requirements for the degree of

Master of Science in Mechanical Engineering

at the

MASSACHUSETTS INSTITUTE OF TECHNOLOGY

June 2014

Author ..... Signature redacted
Department of Mechanical Engineering
May 09, 2014

Certified by... Signature redacted .....
Victor W. Wong
Principal Research Scientist
Thesis Supervisor

Accepted by ..... Signature redacted .....
David Hardt, Professor of Mechanical Engineering
Chairman, Department Committee on Graduate Theses

Development and Application of a Lubricant Composition Model to Study Effects of Oil Transport, Vaporization, Fuel Dilution, and Soot Contamination on Lubricant Rheology and Engine Friction

by

Grace Xiang Gu

Submitted to the Department of Mechanical Engineering
on May 09, 2014, in partial fulfillment of the
requirements for the degree of
Master of Science in Mechanical Engineering

Abstract

Engine oil lubricants play a critical role in controlling mechanical friction in internal combustion engines by reducing metal-on-metal contact. This implies the importance of understanding lubricant optimization at the piston ring-cylinder liner interface. Lubricating oil composition varies along the liner and throughout the engine. Composition changes occur due to degradation, vaporization, mixing during ring passage, fuel dilution, particulate matter contamination, and combustion gases getting onto the liner causing wear and erosion. These chemical and physical properties change oil composition and in-situ oil properties. The objective of this thesis is to discuss the development of an oil composition model to determine rheological properties at critical rubbing surfaces due to oil transport, vaporization, fuel dilution, and soot contamination. This study will specifically focus on the oil on the cylinder liner because the interaction between piston assembly and cylinder wall is where most of the mechanical friction originates.

The first physical process discussed is oil mixing due to piston movement. Axial mixing analysis shows that mixing only occurs when the piston ring is above the oil particle location. Flow rates are calculated at each liner position from using piston speed, film thickness, and pressure gradient parameters. From this basic model of oil transport, chemical processes are applied to each species in each different liner location.

For the process of vaporization, due to high temperatures near the top dead center of the piston, light volatile hydrocarbons vaporize and leave the system. Light carbon number species disappear at a faster rate due to their high volatility and vaporization rates. This results in retention of heavier hydrocarbon species near the top zone of the cylinder liner model. Vaporization rates for different species in each liner location are obtained by looking at individual vapor pressures, mass transfer coefficients, and

other oil properties.

The link between composition and viscosity is a blending equation. The Arrhenius blending equation is used to calculate mixture viscosity from the summation of different species composition and component viscosity values. A combination of composition results shows that near the top dead center or top zone, the viscosity is higher than just considering temperature effects on oil viscosity. The impact of this vaporization component shows that the addition of a non-volatile oil species near the top dead center of the cylinder liner has the ability to flatten the species viscosity versus liner location curve.

Other rheology applications were studied for effects of fuel dilution, additive concentrations, and also soot contamination. This new oil composition model solves for in-situ compositional changes for different oil species due to different physical and chemical processes along the cylinder liner. This change in composition causes a change in viscosity of the overall mixture which is solved for with blending equations. Then from mixture viscosity values, friction and wear can be calculated to optimize the lubricant for fuel efficiency.

Thesis Supervisor: Victor W. Wong
Title: Principal Research Scientist

Acknowledgments

My time here at MIT and the Sloan Automotive Lab has been incredible. There has not been a single day that I did not learn something new either from a classroom, professor, or friend. A number of people have helped make my experience here at MIT more enjoyable and fruitful. I would like to take a moment to acknowledge those who influenced my time here.

I would like to first thank Dr. Victor Wong who gave me the opportunity to work on this project. I learned a lot from him and his expertise in lubrication is unsurpassed. Dr. Wong taught me how to break down problems and think through them in a logical way. He also led me to great resources and always had time to discuss presentations, papers, and research analysis. I am extremely grateful to have had the opportunity to work with Dr. Wong.

Our project partners, Infineum and Kohler. Jai Bansal and Marianne Devine, were essential to the success of my project, giving advice when I needed it most. Bob Linndorfer from Kohler also gave me great insight on my project. I would like to also thank the other project partners who attended our meetings to discuss ideas and data. I would also like to thank the US Department of Energy for their financial support of this program by Cooperative Agreement DEEE0005445, especially Dr. Steve Prezesmitzki and Nicholas Damico who attended our quarterly report meetings.

Several other people from the Sloan Automotive lab have also helped me personally and professionally: Tianshi Fang, Yang Liu, Mathieu Bernier, Camille Baelden, Kevin Cedrone, Tomas Vianna Martins, Mark Moleywk, Mike Plumley, Tim Murray, Justin Kamp, Alex Sappok, Pasquale Totaro, Eric Zanghi, Qing Zhao, Eric Senzer, Michael Bahr, and Kai Liao. I would also like to thank Janet Maslow for doing a excellent job keeping the lab in line and for being a great friend to me over the past two years.

I would also like to thank all my good friends at MIT who have impacted my life and given me a great experience! My friends always made me smile after a rough day and have been a great support system. Leslie Regan, Joan Kravit, and Una Sheehan from the Mechanical Engineering department were extremely helpful during my time at MIT.

I would also like to thank friends from outside MIT, my best friend Claire Wilke for lending a listening ear whenever I needed it and overall wishing me the best. Thank you for always being there for me all these years since elementary school!

Finally, I would like to thank my family for their support. My father who is an impassioned engineer himself for giving me inspiration, my mother who has become my best friend in the world and whose kindness and love is indispensable, my brother who is studying mechanical engineering at Northwestern University and is the most supportive brother I can ask for, and my grandmother who has given me all the love in the world. I am extremely thankful to have such a wonderful family.

Contents

List of Figures

List of Tables

Chapter 1

Introduction

There are many different strategies to improve fuel economy in the automotive industry. One strategy is to use engine oil to generate more efficient running engines. Engine oil viscosity can improve fuel economy when lowered in the formulation. Unfortunately, engine oil viscosity tends to increase during the oil drain interval, which in turn is expected to decrease fuel economy. Lubricant formulation can be designed to resist such changes in viscosity through high quality base oils, antioxidants, and viscosity modifiers. Oil composition is one of the drivers that affect viscosity and therefore can be used as a lever to improve fuel economy of the engine.

High temperatures in the combustion chamber cause light/volatile hydrocarbons to vaporize and leave heavy hydrocarbons behind near the top dead center of the cylinder liner, resulting in oil composition variations in the power cylinder. Accumulation of heavy hydrocarbon oil near top of cylinder liner causes the viscosity to increase, showing that oil composition has effects on oil properties and friction. This paper will discuss the development of an oil composition model to determine lubricant composition due to interactions of contamination, vaporization, oil transport, and mixing on the surfaces of the piston and cylinder liner. The method of obtaining composition of a lubricant involves using different engine zones, different species, mass mixing rates, and physical and chemical processes as inputs. The model reports composition at different spatial locations and how it evolves with time. From composition, rheological properties such as viscosity can ultimately be determined at

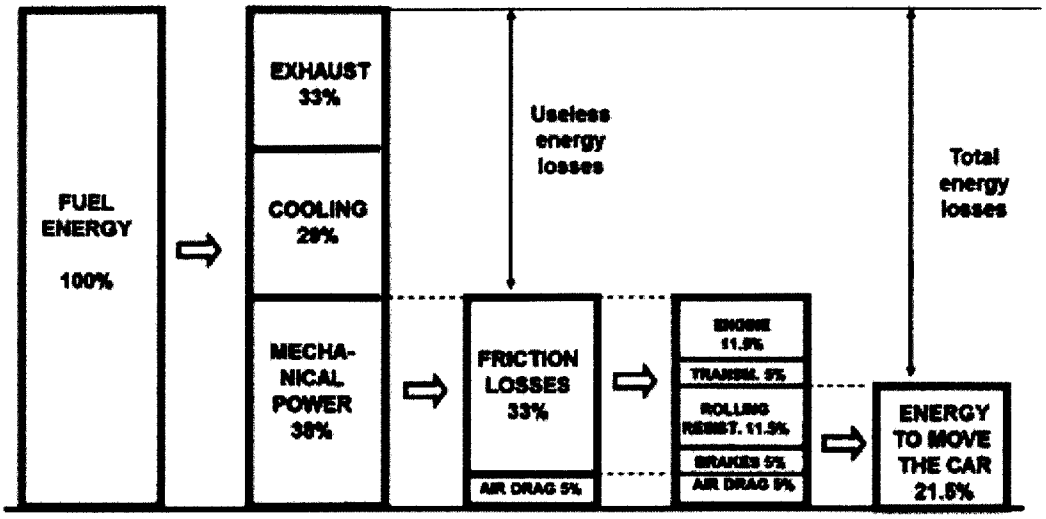

Figure 1-1: Passenger car energy consumption breakdown shows 38% of fuel energy used for mechanical power to overcome friction and air drag [11]

critical rubbing surfaces. Viscosity can then be utilized when attempting to lower the friction in the engine.

1.1 Importance of Friction on Engine Efficiency

Due to strict fuel economy requirements for the development of modern internal combustion engines, engine efficiency needs to be constantly improved. Improvement in engine efficiency in automobiles requires reduction of energy losses from exhaust, cylinder cooling, and mechanical losses. Mechanical power accounts for 38% of fuel energy use in an engine (Figure 1-1), where some of it used to overcome engine friction losses of 11.5%. Of the friction losses from the engine, 45% of it originates from piston ring-pack and cylinder liner assembly (Figure 1-2). Piston ring assembly is the area where almost half of the friction occurs and is definitely an area studied in terms of lowering friction. The rest of the energy losses lies in the valvetrain and auxiliary losses from operation of pumps and other engine operation components. As a result, decreasing mechanical friction provides opportunities in improving fuel economy [11].

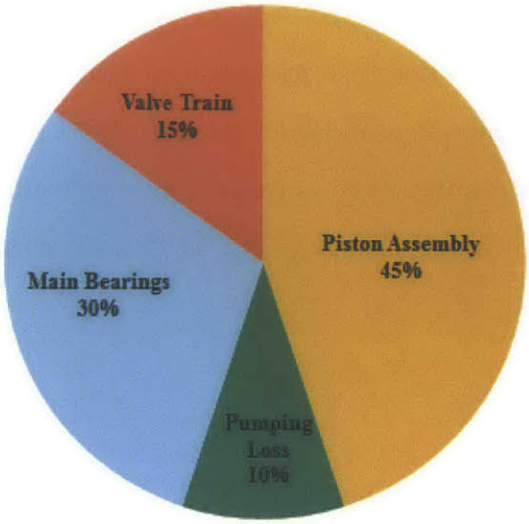

Figure 1-2: Roughly half of energy loss from piston ring-pack zone from engine friction losses

1.2 Optimizing Lubricant Formulation

Engine oil lubricants play a critical role in overcoming mechanical friction in internal combustion engines by reducing metal on metal contact. This draws attention to the importance of understanding how to optimize lubrication at the piston ring-cylinder liner interface.

Lubricants consists of a base oil and various additives, which protect the engine and reduce the rate at which the engine oil degrades. Additives improve the performance of oil, increases its useful life, and add wear protection. Base oils make up most of the lubricant and additive packages typically account for 20-30% of the formulation and contain detergents, dispersants, pour-point depressants, viscosity modifiers, friction modifiers, and anti-wear compounds (ZDDP). Dispersants help keep degraded oil from coagulating, so that the coagulated oil will not be able to block narrow lubricant passageways. A pour-point depressant allows the oil to flow at low temperatures. Viscosity modifiers help reduce a lubricants change in viscosity subject to changes in temperature. Modifiers consist of polymers and copolymers which uncoil at high temperatures to increase viscosity. ZDDP inhibits oil oxidation and protects

against wear [18].

Optimizing a lubricant to decrease friction and wear can be beneficial due to increasingly strict engine emission standards. This study focuses on how an oil composition model can help determine what factors change the composition of the lubricant and the implications of it on oil rheology and friction to optimize the lubricant.

1.3 Motivation

Due to all the complex processes that can occur in the combustion chamber, compositional effects from these chemical and physical processes on oil viscosity are not studied much and are unknown. Temperature effects on oil viscosity, however, is well understood. It is a well-known fact that temperature changes the viscosity of the oil. As the temperature increases, the viscosity decreases either using the famous Walther or Vogel Equation [19]. Figure 1-3 shows the temperature effects on kinematic viscosity using Vogels equation for two different oils, SAE 10W30 and SAE 15W40. There is an order of magnitude difference along the liner due to temperature variations from 80°C to 200°C. However, it is important to note that oil composition will also change oil viscosity, which is why it is important to study both compositional and temperature effects on oil rheology.

Lubricating oil composition varies along the liner and throughout the engine and can be used to solve for rheological properties of oil at critical rubbing surfaces. Composition changes occur due to degradation, vaporization, mixing during ring passage, fuel dilution, particulate matter contamination, and combustion gases getting onto the liner causing wear and erosion. In addition, an oil composition model can predict the TBN or total base number of the oil. TBN measures the lubricants basicity, which aids in the control of acids formed during the combustion process. Oil is continuously exposed to acidic combustion gases, so controlling the base number is necessary to prevent the corrossion of the upper piston, piston rings, top end bearing and even valvetrain. Low TBN is related to reduced oil detergency and high basicity is related to lowered oil performance. A balance is therefore necessary to guarantee a

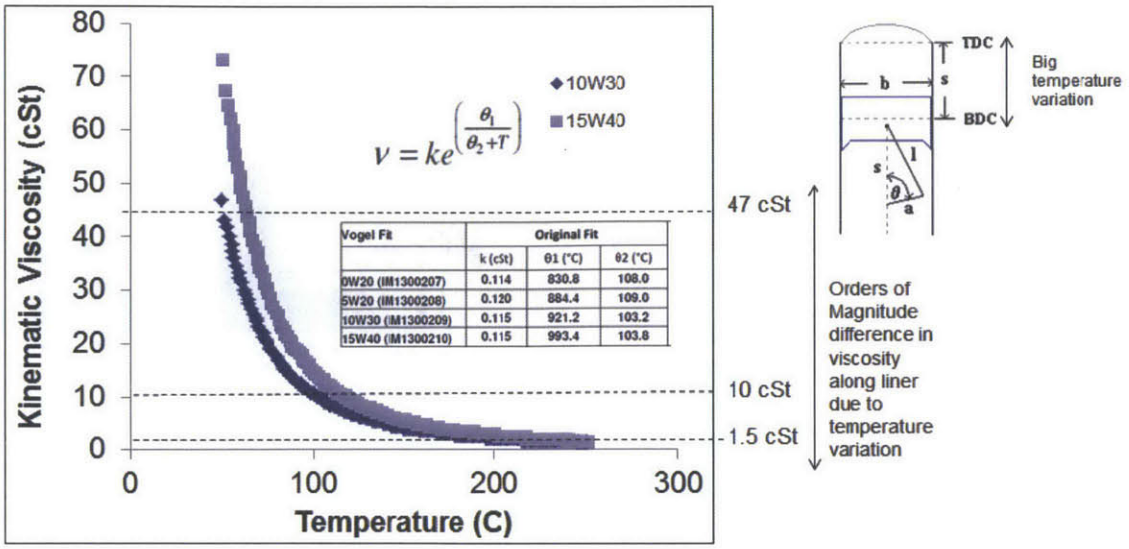

Figure 1-3: Increase in temperature causes decrease in kinematic viscosity of oil

well-maintained engine [3]. These chemical and physical properties change oil composition and in-situ oil properties. To sum up, the process is complicated and needs to be organized in an oil composition model. An oil composition model is created to account for some issues to better understand how to optimize the lubricant to take into account compositional effects on oil properties to reduce friction and wear.

1.4 Composition Modeling Background

The effects of compositional changes due to vaporization have been studied by a few authors, including Audette, Liang, Cho, and Yilmez [3][5][26][14]. These authors focused on oil transport and vaporization as a base for their model. None of these authors connected their research to oil rheology from composition, which is the basis of this research.

Audette presented a detailed derivation of the equations governing the instantaneous evaporative heat flux of a species as well as a model for estimating vaporization and composition changes along the liner. He showed that the amount of vaporization from the liner is about 1.3 g/hr/cylinder, or about 10% of the total oil consumption

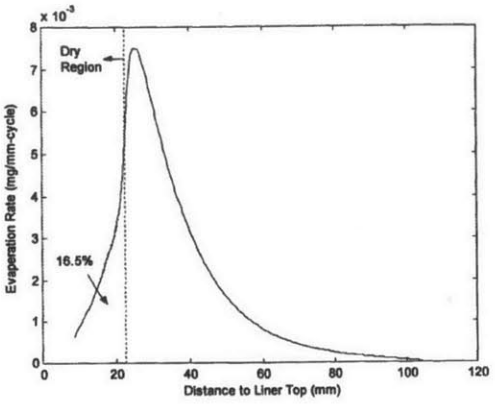

Figure 1-4: Distribution of evaporation rate along liner highest for region close to after TDC [14]

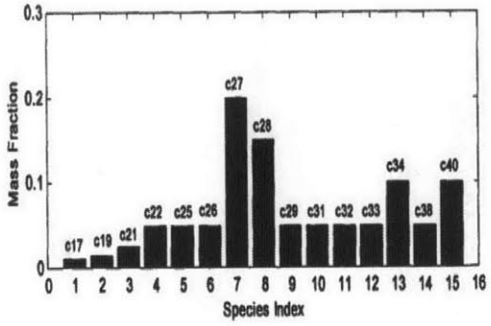

Figure 1-5: Composition of synthetic oil for various species [14]

expected for the engine. He also discovered that vaporization is strongly dependent on liner temperature, steady state oil composition, and the parameters used internally to model the mass convection coefficient [3].

Liang created a model to estimate the effects of oil evaporation on the liner on oil consumption for a light diesel engine. He used the composition of synthetic oil with various carbon numbers and mass fractions depicted in Figure 1-5. His results showed that the total evaporated oil over a complete cycle was 0.175 mg, with the four lightest species adding up to 70% of the evaporated oil. The distribution of evaporation rate along the cylinder liner, the region around the lower range of the dry region, has the highest evaporation rate and contributes most to total oil evaporation (Figure 1-4). Inside the dry region shown in the figure, although the liner temperature increases as the axial location gets closer to the liner top, the evaporation rate decreases because it becomes more difficult for fresh oil to be transported into the upper region. The fresh oil is easier to reach and lubricate near the lower bound of the dry or starved region [14].

Yilmez also discussed composition changes due to volatility of oil [26]. He mentions that higher piston temperatures reduce the oil viscosity, and therefore may change the oil transport along the piston. Moreover, higher liner temperatures will increase oil evaporation. His experiments showed that the lightest oil species was found to

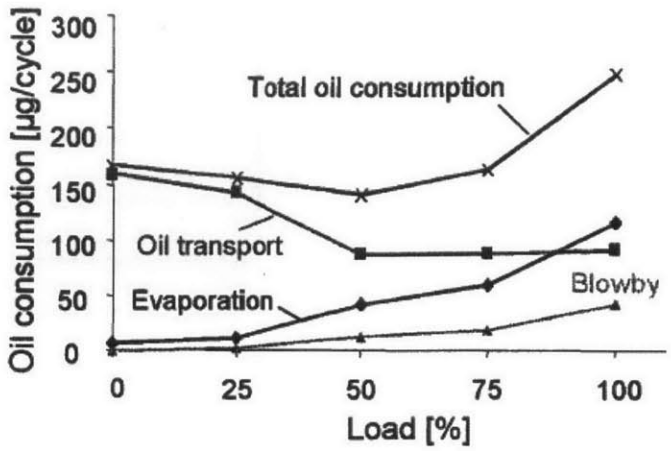

Figure 1-6: Effect of engine load on different consumption sources and on total oil shows different contributions of oil transport, evaporation, and blowby [26]

contribute around 35% to the total oil evaporated. The four lightest constituents make up almost 80% of the evaporated oil, which is a significant amount. Therefore, because of the limited oil supply and the evaporation of lighter species at severe high load and liner temperatures, fresh oil from the sump may not be able to refresh the oil over a larger region of the liner in each cycle. At high liner temperatures, volatile species of the oil on the liner deplete due to high evaporation rates. Then the oil composition on the liner may change and differ from the oil composition in the sump. This change in composition of the oil on the liner is governed by the ring liner lubrication oil transport rates along the liner, and by the evaporation rate from the liner. Yilmez also remarks that oil consumption is made of three main things: oil transport, evaporation, and blowby (Figure 1-6).

Cho created a liquid oil transport model that integrated oil vaporization to investigate the change of oil composition on the crown land with each engine cycle for different hydrocarbon species shown in Figure 1-7 and Figure 1-8 [5]. He also determined in his modeling that during the engine cycle, there is a significant increase of heavy oil components while the light fractions tend to decrease and the medium heavy oil components stay relatively constant.

Wahiduzzaman developed a model for oil consumption due to in-cylinder evap-

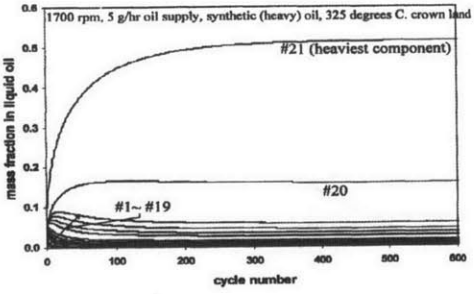

Figure 1-7: Mass fraction of liquid oil calculated at the start of every cycle shows highest for heavier species [5]

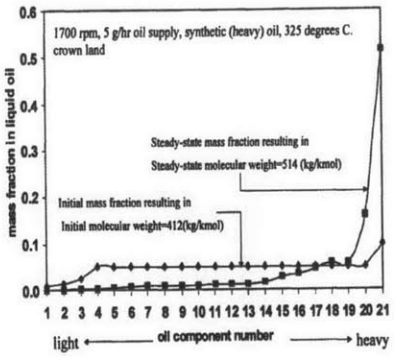

Figure 1-8: Mass fraction after steady state for heavier species is greater than initial composition [5]

oration of oil in reciprocating engines [24] . The model is based on conservation of mass and energy on the surface of the oil film left on the cylinder by a piston ring pack. He discusses transport and oil consumption methods :

1. Transport

   (a) Accumulation of differential oil scraped up and down by rings

   (b) Oil scraping: Oil film left by ring pack on cylinder

   (c) Entrainment of oil into and dispersed oil flow with inter-ring gases

2. Throw-off

   (a) Throw-off of oil accumulated above top ring due to inertia effects

   (b) Evaporation from oil film on cylinder surface

   (c) Return into cylinder of oil mixed with inter-ring gases

These specific authors employ methods that describe oil transport and evaporation which are involved with studying changes of composition. Since other chemical and physical processes are not coupled in this composition literature, there is more to study and understand in a more complete version of what is happening to cylinder liner oil during engine operation.

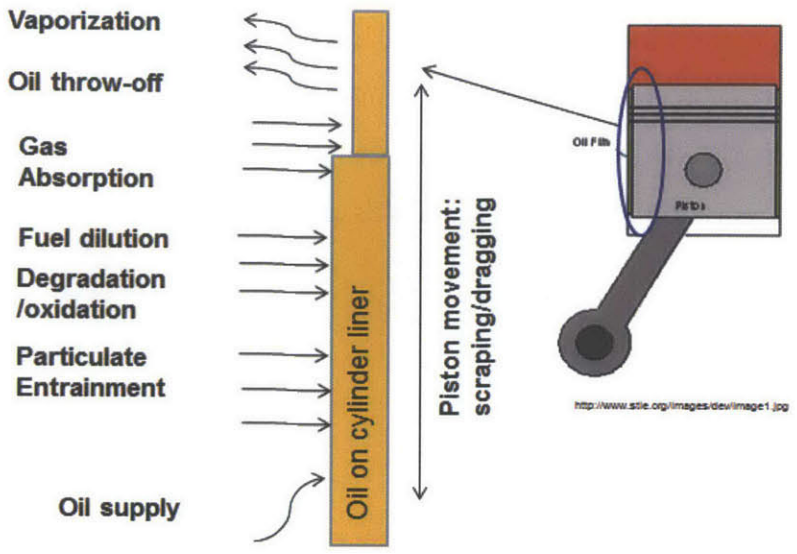

Figure 1-9: Processes that change oil composition in time and space add complexity to model

1.5 Extended Applications

Most of the composition background included applications such as oil transport and vaporization. However, what sets this research apart is the extended applications in addition to oil transport and vaporization. The modeling of fuel impingement and soot contamination is unique and has not been done in literature as of yet. Empirical studies of soot contamination and fuel dilution on oil viscosity exists, but the coupled modeling of these processes does not. This study presents many extended applications of the oil composition model and couples many different processes (Figure 1-9). It is important to have a more complete model of what is going on in the combustion chamber because some processes can have a big effect on the rheology of oil and cannot be left out.

Chapter One discussed the motivation and some background research concerning existing composition models. Chapter Two describes the modeling procedure to calculate composition of species in different areas within the engine. It will discuss oil transport due to piston movement. Chapter Three addresses the modeling approach of vaporization process. Chapter Four covers the base calculation of viscosity through blending equations. Chapter Five introduces the connection between composition and

viscosity through the blending equation. Chapter Six discusses the applications of additive concentration, fuel impingement, and soot contamination. Results for each applications are discussed in detail as well. Chapter Seven presents a summary of the results and also potential future work for this model.

Chapter 2

Model Description

As a first step in modeling the composition of the oil, the engine oil was modeled as being composed of several distinct paraffin hydrocarbons. The cylinder liner oil is focused on and divided into several regions. Details of the base modeling approach is discussed in this chapter. Engine Specifications for the Department of Energy (DOE) project engine is introduced first.

2.1 Engine Specifications

The main goal of the program is to optimize lubricant formulations to enhance engine efficiency in modern internal combustion engines. The program is split into three phases and involves optimizing different subsystems of the engine. The author works on optimizing the power cylinder subsystem.

The engine used in this study is a light-duty Lombardini engine supplied from Kohler (KDW702 model). It is approximately 700 cm^3 with peak cylinder pressure of 50 bar and engine parameters shown in Table 2.1. The lubrication circuit for the Kohler engine is shown in Figure 4.1. In terms of the lubricant used in this engine, Lombardini recommends that lubricating oil viscosity be selected based upon the highest temperature expected. In normal applications, the lubricating oil viscosity selection is based upon the seasonal temperature ranges expected for the engine geographical territory. The use of straight weight lubricating oil such as SAE 40, SAE

Parameters	Value	Units
Bore	75	mm
Stroke	77.6	mm
Displacements	686	cm^3
Compression ratio	22.8:1	n/a
Speed	3600	RPM
Cylinders	2	No.
Maximum Torque	37	Nm
Oil comsumption	9	g/hr

Table 2.1: Engine specifications for Kohler KDW702 engine

30 is not recommended for Lombardini diesel engines.

2.2 Engine Oil Modeling

Engine oil is composed of base stocks and additives. Base stocks are the main constituent of the engine oil and are generally hydrocarbons, which are either paraffinic, naphthenic, or aromatics. Additives constitute up to 20% of engine oil and contain hydrocarbons and metallic components [10]. This section discusses the inputs of initial oil composition and zones of this composition modeling.

2.2.1 Initial Oil Composition

Lubricants are a complex mixture of components that are used to maximize the level of protection to engine components. They consists of a hydrocarbon base oil, viscosity modifier, and an additive package. The base oil alone cannot provide all the functions required and additives make up what base oils cannot do.

Species in the model could include anything that makes up the oil. Species could include hydrocarbon base oil which is composed up carbon and hydrogen. The American Petroleum Institute designates several types of lubricants in Groups I, II, III, IV, and V. Base oil can also be classified as paraffinic, naphthenic, and aromatic. Specific types of paraffins include alkanes and alkenes.

Viscosity modifiers are designed to reduce a lubricant's change in viscosity when

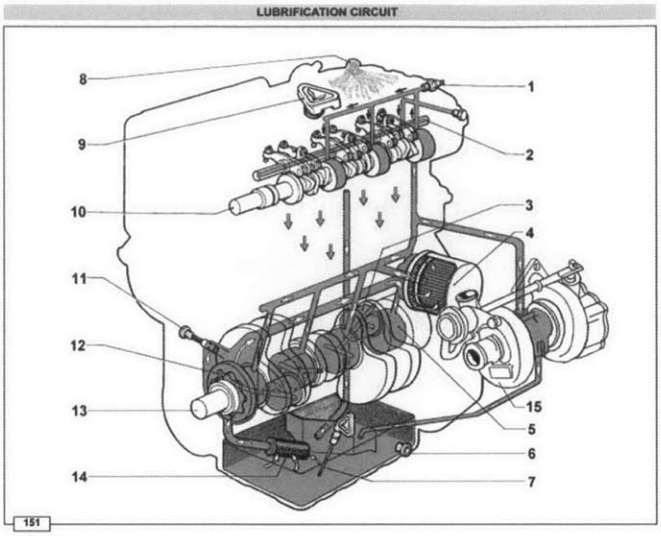

Figure 2-1: Lubrication circuit for Kohler KDW702 engine (from Kohler engine manual)

subjected to changes in temperature. One type of viscosity modifier is olefin copolymer (OCP) which usually consists of molecular weights in the 70,000 g/mol range, which is vastly greater than the ranges of 100-200 g/mol for hydrocarbons [15].

Additives serve to protect the base oil and examples include dispersants, antiwear additives, friction modifiers, and detergents. These additives contain different elements that can also be modeled as a species such as calcium, magnesium, zinc, phosphorus, barium, sodium, lead, and potassium [25]. An oil composition model with the right input parameters for different species in the oil can track the compositional changes in space and time of all oil species.

2.2.2 Model Specific Initial Oil Composition

For this model, the base initial oil composition is modeled as a compound of several different paraffin hydrocarbon components with different liquid-phase mass fractions and boiling points. Properties such as molecular weight, vapor pressure, and gas-phase mass fraction of each oil component were then obtained in order to calculate

the vaporization rate of each oil component from the liquid oil film.

Mass fractions in the liquid oil and boiling points of synthetic and mineral oil corresponding to the points on the distillation curve. This is the initial composition in each zone on the cylinder liner. The initial composition contains equal fractions of each alkane in each zone and the zones in detail are discussed in the next subsection. The base oil composition will be made up of serveral paraffins. With different applications, this oil package is tweaked to fit a certain criteria which will be shown in Chapters Five and Six in which specific applications will be discussed. If additives are added, they will be added of a lesser amount than the pure hydrocarbons.

2.3 Engine Zonal Modeling

In addition to inputting species information into the model, other inputs include which zones inside the engine are considered. This section discusses the possible zones that could be modeled and which ones specifically will be discussed in the following chapters.

2.3.1 Zone Definition

Zones used in a composition model could be any subsystem within the engine. Such areas could include valve-train, piston ring pack, bearings, crankshaft (Figure 2-2). Due to different operating conditions, oil composition in all these different zones is different. For instance, the valve-train does not experience the same harsh operating conditions as the piston ring pack and therefore does not experience vaporization or fuel dilution. The temperature range for valvetrain is around 100°C while that of the power cylinder is approximately 200°C. The valve-train also contributes about 15% of total friction while that of the piston ring pack contributes to about 45% of the total friction.

For this model all these different zones communicate with each other. The sump brings fresh oil to the piston ring pack and also sends oil to the valve-train system. The valve-train and power cylinder drip oil back into the sump. This communica-

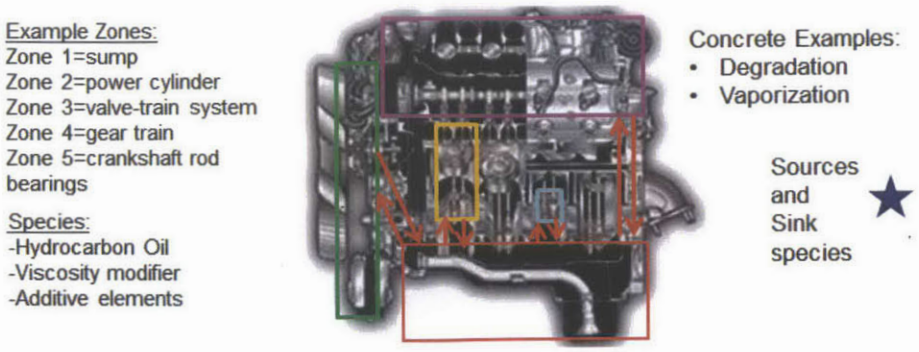

Figure 2-2: Different zones in the engine communicate with each other

tion causes contaminated oil from the piston ring pack to be sent to the valve-train. Different zones are used to track how the composition of the species change through time and space.

2.3.2 Focus on Ring Pack Zone

The focus of this thesis in terms of zones will be within the power cylinder ring pack zone. Of all mechanical friction within the internal combustion, 40-60% occurs because of the interaction between the piston assembly and the cylinder wall, with a large proportion occuring at the top compression ring/cylinder liner interface. This interface is purposely almost starved of lubricant in order to control exhaust emissions. As a result, facilitating friction reduction at this location is incredibly difficult.

This zone is also focused on because this is where most volatile losses occur (Figure 2-3). This area is also where the most oil is needed. Shown below is a schematic of the volatile losses that originate mostly from the ring pack block instead of the crankcase block [25]. For this model, the cylinder liner oil is focused on and split into ten zones (Figure 2-4). The first zone being the area on the liner that is closest to the top dead center (TDC), and the last zone being the area on the liner closest to the bottom dead center (BDC). Each zone has a certain fraction of different species and the addition of all fraction of each species in each zone will add up to one.

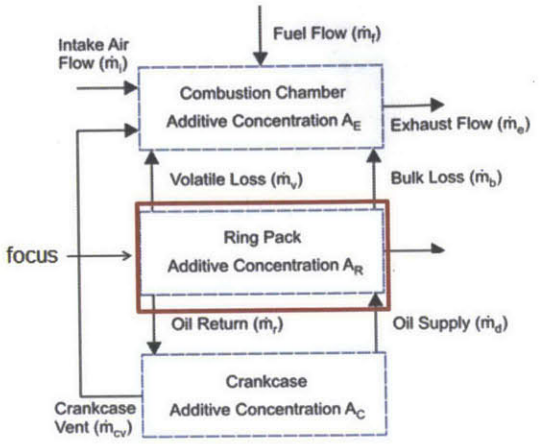

Figure 2-3: Volatile Loss mostly originating from ring pack zone and not from crankcase or combustion chamber [25]

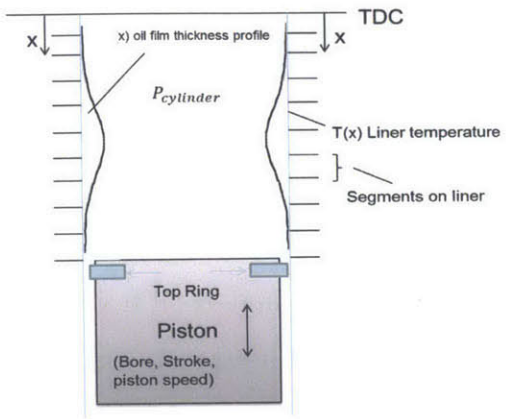

Figure 2-4: cylinder liner oil divided into individual different zones to determine composition at each position

$$\frac{dm_i^{(k)}}{dt} = \underbrace{-Y_i^{(k)} \sum_{j=1}^{L} \dot{M}_{i,j}}_{\text{Outgoing mass flow}} + \underbrace{\sum_{j=1}^{L} Y_j^{(k)} \dot{M}_{j,i}}_{\text{incoming mass flow}} + \underbrace{source_i^{\,k}}_{\text{Species generated}} - \underbrace{sink_i^{\,k}}_{\text{Disappeared species}}$$

Figure 2-5: Composition equation to solve for change in mass m, depicting variables i for the current zone, j for the zone in front of the current zone, k for the specific species

2.4 General Equation for Oil Composition Model

The general equation for the oil composition model uses mass balance in which there is outgoing and incoming mass flow due to piston movement (Figure 2-5). When mass is transferred, the composition of the previous zone gets moved to the new zone. There is also a component of the species generated or the 'source' term such as degraded species due to the process of degradation and disappeared species or the 'sink' term such as the process of vaporization. During the process of vaporization, light hydrocarbon species disappear and act as a sink term due to the high temperatures near top dead center. This equation can be extended to many other applications such as fuel dilution, combustion gas absorption, and also soot contamination. Fuel impingement on the cylinder liner is a source to the zone because it is adding fuel to the system. Soot getting into the oil is also a source for the zone. In the rheology and applications Chapter Five and Six, this equation will be utilized to calculate the new oil composition over time for a specific species in a specific zone on the cylinder liner.

Chapter 3

Oil Transport

During an engine cycle, the composition of the oil film on the liner changes due to evaporation and ring passage. The calculation of the change of oil composition due to ring passage is associated with the lubrication of the piston ring-pack. The ring pack consists of three rings: top ring, scraper ring, and oil control ring. All three rings serve different purposes. The top two rings help control blow-by and regulate the gas flows in the ring pack. The oil control ring controls the oil film thickness left on the liner, which lubricates the top two rings and plays a role in controlling engine oil consumption.

The piston rings move up and down the cylinder liner are one method of oil transport. There are actually many mechanisms that cause liquid oil to be moved around in the Piston-Ringpack-Liner system (Figure 3-1). Driving mechanisms include inertia, ringpack gas flows, pumping motions by rings, scraping of oil from the liner by the rings, and carrying of oil along the liner by the rings. Paths for oil transport include transport along piston lands, through ring gaps, into and out of ring grooves, and along the cylinder liner [3][26]. Given that several mechanisms can drive oil along each of the several paths, quantifying oil transport in this system is very complicated. This chapter will discuss the oil transport component of the model which includes an understanding of oil film thickness, oil displacement, and flow rates.

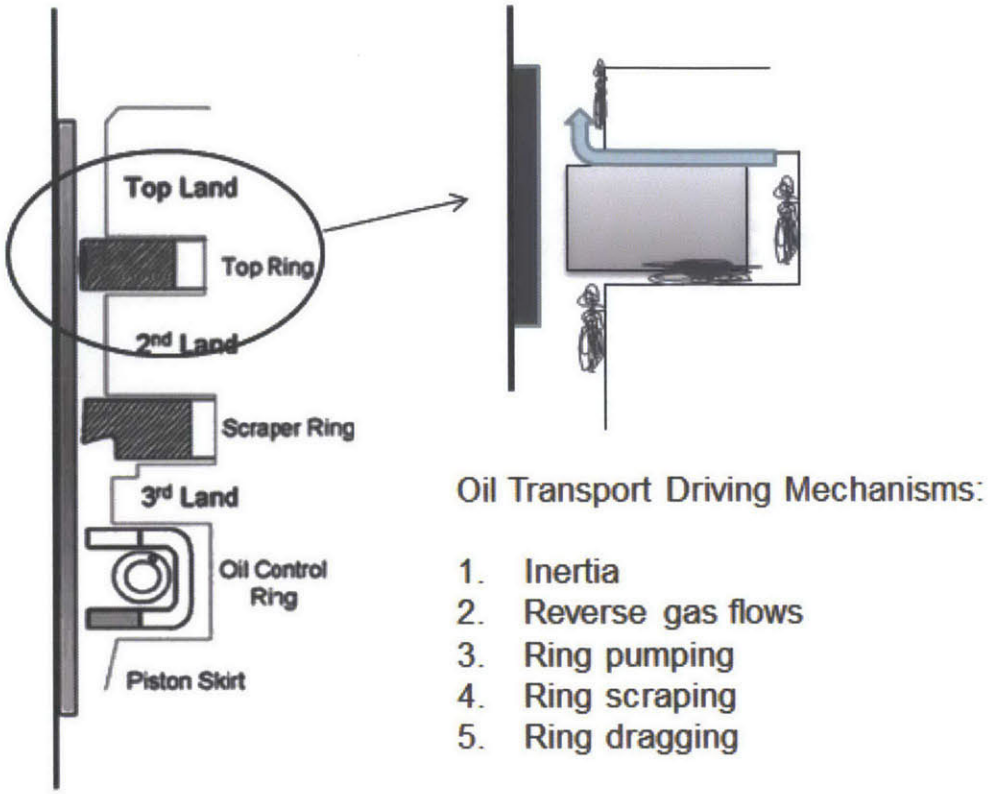

Figure 3-1: Mechanism for oil transport zoomed in on top ring and includes different driving mechanisms [3]

3.1 Oil Transport Due to Piston Movement

Scraping and dragging of oil on the cylinder liner are two mechanisms of oil transport. Dragging occurs because oil attaches itself to the ring face as the ring moves up and down the liner (Figure 3-2a). The oil attachment occurs because it is assumed that there is a no-slip condition between the oil layer and the ring face. As a result, oil is dragged up and down the liner as the ring itself moves up and down the liner. At any given moment in time, a certain volume of oil is trapped under the ring face and is being carried with the ring. To calculate the amount of oil attached to the ring face (and, therefore, oil transported by carrying), calculate the volume of oil under the ring face and then, to account for the amount of oil not moving with the ring face, subtract off the volume of oil left on the liner after the ring passes. The remaining volume is defined as the carried oil.

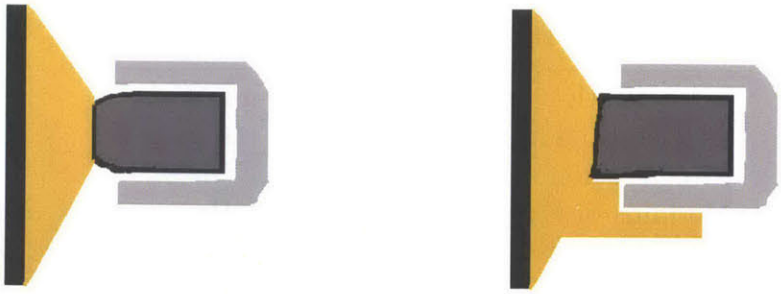

(a) Dragging due to piston movement carries oil from one region of the cylinder liner to another

(b) Scraping of oil is the accumulation of oil in front of the ring and scraps it to another region

Figure 3-2: Oil Transport Methods

Scraping occurs when the oil on the liner floods the leading edge of the ring face (Figure 3-2b). Scraping rate is the rate of oil being removed from the cylinder liner when the leading edge is flooded minus the change in volume being dragged [3]. Due to the complexity of scraping, dragging will be the main mechanism discussed in this model. An addition of scraping mechanism can be included in the future model. Preserving oil mass conservation ensures a precise oil transport simulation and lays a solid base for oil transport and oil consumption analysis. Conservation of mass will be discussed along with lubrication theory, oil displacement, oil film thickness, and oil renewing.

3.2 Top Ring Oil Film Thickness

To calculate oil displacement and flow rates, oil film thickness at each crank angle is an essential input. To calculate oil film thicknesses, a fully flooded model for the top profile ring is modeled and analyzed first. A fully flooded model assumes that the wetting area is the entire ring width. This specific model will tend to overestimate oil film thickness underneath the ring and therefore oil consumption. This section will discuss the development of a fully flooded ring model and then the next section will discuss the modeling of a starvation model.

Profile Ring Parameters	Value	Units
Ring Width	2	mm
Surface Roughness	0.1	micrometers
Ring Tension	10	N
Modulus of Elasticity	200	GPa
Poisson's Ratio	0.285	n/a

Table 3.1: Top ring parameters used to solve for different forces in ring balance

3.2.1 Top Ring Parameters

All three rings have different parameters. The top ring parameters are shown in Table 3.1. These parameters will come into use when determining the contact force, tension force, and hydrodynamic force.

3.2.2 Force Balance

To solve for the top ring film thickness profile, the force balance for the top ring needs to be studied (Figure 3-3). The different forces that act on the top ring include contact force, hydrodynamic oil force, gas pressure force, and tension force. These forces will be discussed below in more detail. After the forces are solved for each crank angle, the model checks if these forces all add up to zero, and if it doesn't, the program iterates through by trial and error with different film thickness values.

Contact Force

The contact pressure is solved by using Greenwood Tripp's contact model for the given ring parameters such as surface roughness [9]. The final equation for contact pressure uses the integrated contact pressure across the ring profile, in which is shown in the equation below:

$$h = 8.284(x - 0.001)^2 + h_0 \tag{3.1}$$

where h is the height at a certain x coordinate and h_0 is the height underneath the ring or the minimum film thickness. At each crank angle, a minimum film thickness will be guessed and plugged into this equation to iterate through the program.

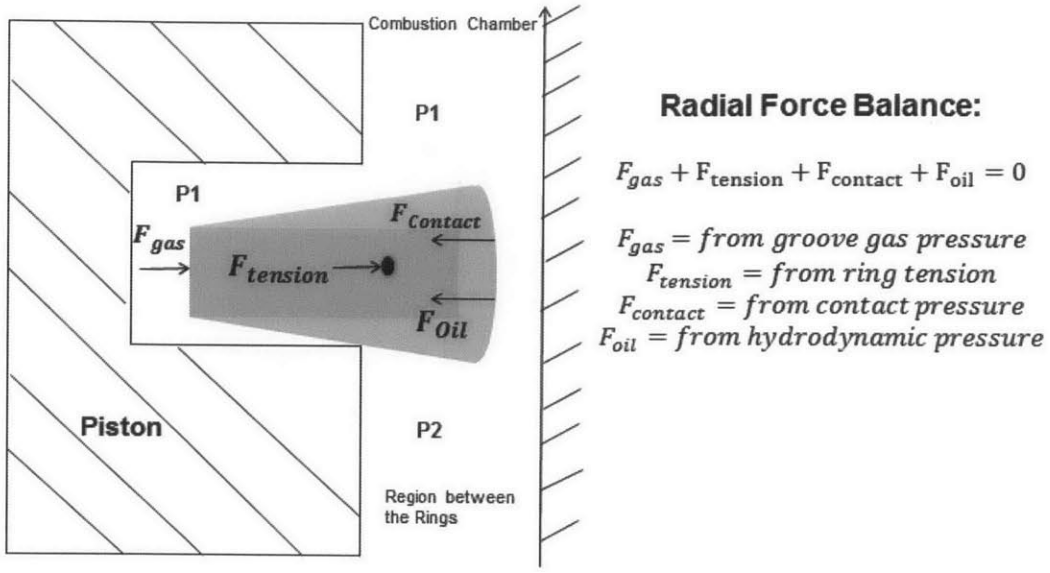

Figure 3-3: Force balance between contact force, hydrodynamic oil force, gas pressure force, and tension force

Hydrodynamic Oil Force

The hydrodynamic pressure is solved for using the Reynold's equation in the method similar to what Tian employed [21]. The pressure is integrated across the ring profile following a similar method used in the contact force calculations. The greater the hydrodynamic oil pressure, the greater the film thickness. The curved profile of the top ring gives it higher hydrodynamic oil pressure as opposed to having a flat profile.

Gas Pressure

The gas pressures are shown as $P1$ and $P2$ in the force balance. $P1$ is the pressure in the combustion chamber and $P2$ is the pressure in the region between the rings. The pressure curves for both pressures are shown in Figure 3-4. It is assumed that $P1$ dominates and that the ring resides on the bottom of the groove at most crank angles. The gas pressure force is represented as $F_{gas} = P1 \times B \times \pi \times Bore$, where B is the ring width and $Bore$ is the bore of the piston.

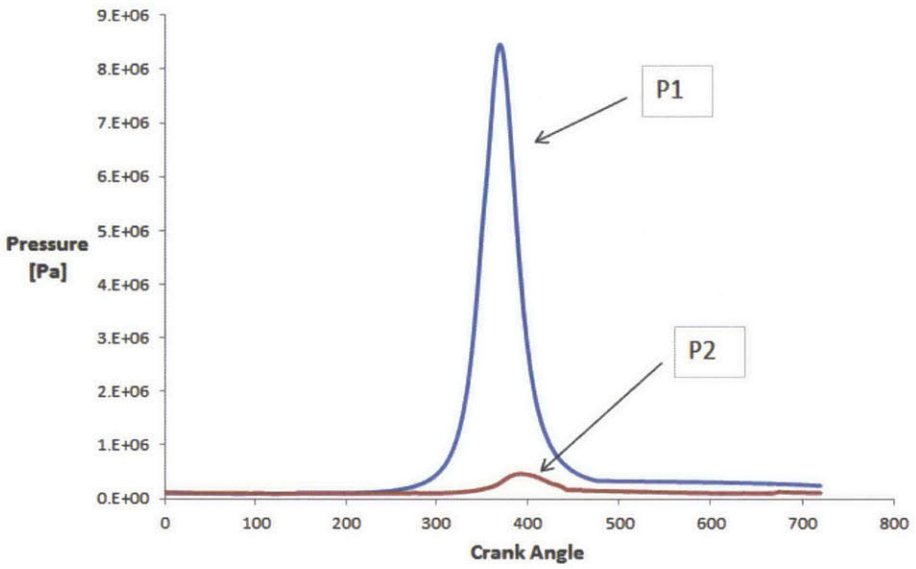

Figure 3-4: Combustion gas pressure $P1$ and pressure in region between the rings $P2$

Tension Force

The tension force is represented as $F_{tension}$ in the force balance diagram. The greater the tension force in the top ring, the smaller the film thickness. The ring tension for the top ring is 10 N. Therefore the total tension force is a constant and is a total of $10 \times 2 \times \pi$.

3.2.3 Fully Flooded Top Ring Results

Top ring results are shown in Figure 3-5. Using a variation of surface roughness, it can be noted that the hydrodynamic regime of lower surface roughness is higher than that of the higher surface roughness. The hydrodynamic regime is usually the regime greater than 4 times the surface roughness. For instance, with a surface roughness of 0.1 micrometers, the hydrodynamic regime is the film thickness greater than 0.4 micrometers of film thickness. During the power stroke, there are lower film thicknesses due to the high gas pressures during combustion. The other three strokes have relatively similar minimum film thickness under the ring. The next section will discuss a starvation model in which the wetting area of oil underneath the piston ring is not the entire ring width, but is only a portion of it.

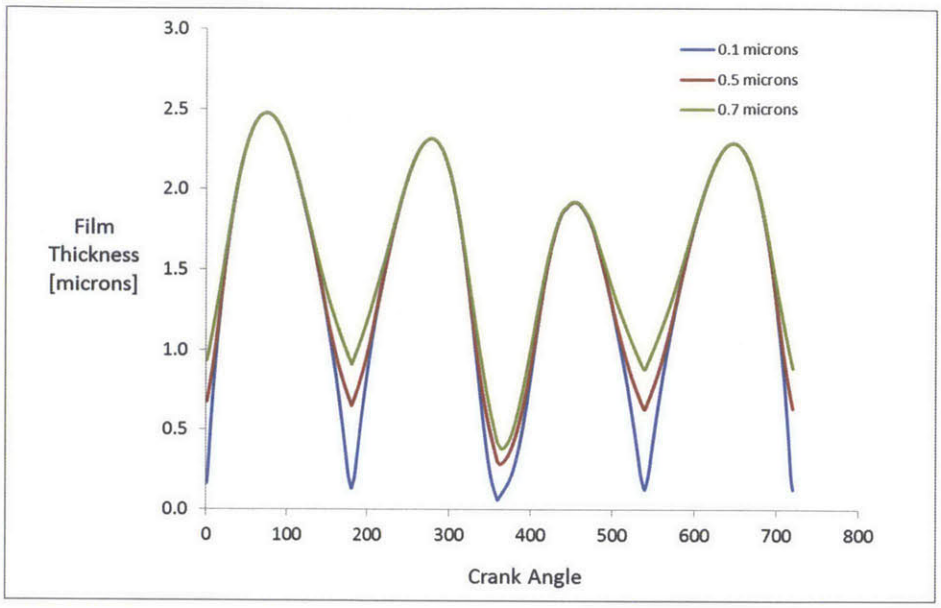

Figure 3-5: Fully flooded top ring film thickness model shows increasing hydrodynamic regime with decreasing surface roughness

3.3 Starvation Model

For the fully flooded model shown earlier, it is assumed that the entire area underneath the top ring is exposed to oil. In reality this does not happen, hence a starvation model is also analyzed. To develop such a model, the oil control ring also needs to be studied in addition to the top ring. Chen developed correlations for the top ring and also the oil control ring hydrodynamic oil pressure [4]. This section will discuss parameters used for the oil control ring, correlations used for hydrodynamic oil force, and results for the starvation model.

3.3.1 Oil Control Ring

Oil control ring profile is different from that of the top ring. It no longer has the curved profile of the top ring that gives it higher hydrodynamic pressure. Additionally, it does not have gas pressure because it is assumed that the top ring does a good job in sealing the combustion gases. As a result, the only forces on the oil control ring are tension force, hydrodynamic force, and contact force. The tension force used for the oil control ring is 20 N. The contact model is the same as the top ring without the

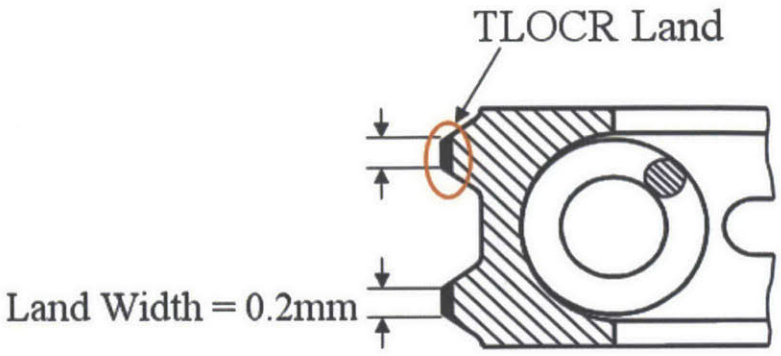

Figure 3-6: Oil control ring has a flat profile as opposed to top ring's curved profile [4]

curved integrated profile. The hydrodynamic pressure closely follows the correlation and parameter's used in Chen's model [4]. In addition, the top ring's hydrodynamic oil profile also uses the correlation in Chen's modeling, in which case one of the input parameters is the oil control ring film thickness as the oil supply to the top ring.

3.3.2 Oil Film Thickness Results

The oil control ring minimum thickness and top ring's minimum thickness profile are calculated from the methods discussed above (Figure 3-7). Looking at the oil control ring results, all the profiles look relatively similar as opposed to the top rings oil film thicknesses. The reason for this is the lack of gas pressure acting on the ring for the oil control ring. It is assumed that the top two rings do a good job sealing the combustion gases. At most crank angles, the oil control ring film thickness is greater than that of the top ring because it acts as an oil supply to the top ring. Again, the top ring has smaller power stroke film thickness values because of the high gas pressure during combustion.

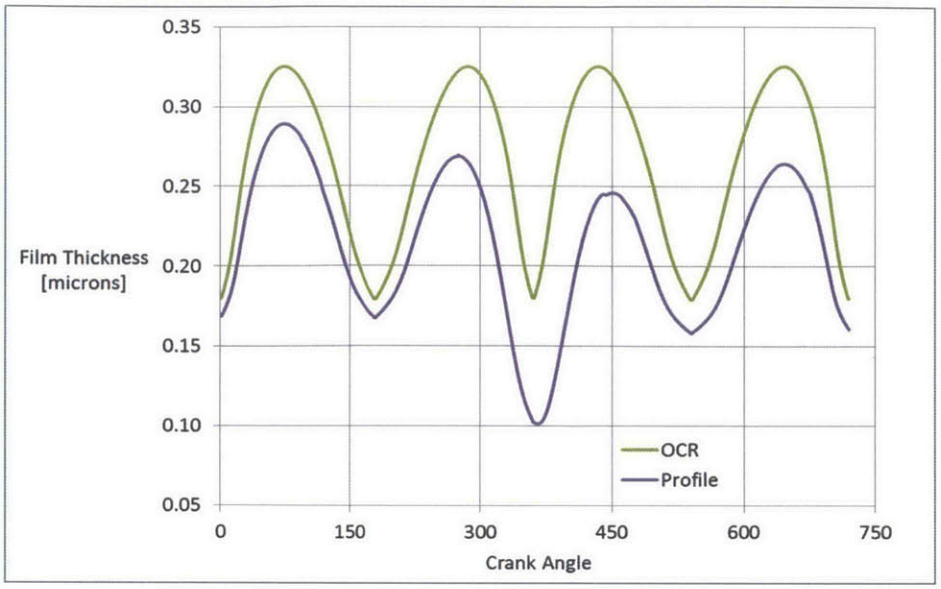

Figure 3-7: Starvation model shows lower film thickness for top ring than fully flooded model

3.4 Leading and Trailing Heights

To determine the leading and trailing heights, control volume analysis was used (Figure 3-8). The box highlighted on the left of the figure is the control volume 1 and the box highlighted on the right of the figure is the control volume 2. The trailing height, $h_{trailing}$, is the height of the oil behind the ring when the ring passes a certain position and $h_{trailing}$ is the height of oil in front of the ring. The equations to solve for the heights are shown below:

$$\begin{aligned} \dot{m}_1 &= V_p \cdot h_{trailing} - V_{average} \cdot h_{ring} = \frac{\partial h}{\partial t} \cdot \frac{ring - width}{2} \\ \dot{m}_2 &= -V_p \cdot h_{trailing} + V_{average} \cdot h_{ring} = \frac{\partial h}{\partial t} \cdot \frac{ring - width}{2} \end{aligned} \tag{3.2}$$

$$V_{average} = \frac{V_P}{2} - \frac{1}{\mu} \cdot \frac{\partial P}{\partial x} \cdot \frac{h_{ring}^2}{12}$$

where $\dot{m}_1$ and $\dot{m}_2$ are the control volume change in mass quantities, V_p is the piston velocity, $V_{average}$ is the average velocity at the location right below the ring tip, h_{ring} is the height underneath the tip of the ring, $\frac{\partial h}{\partial t}$ is the change in height over time, $ring_{width}$ is the width of the ring, which in this case is 2 mm.

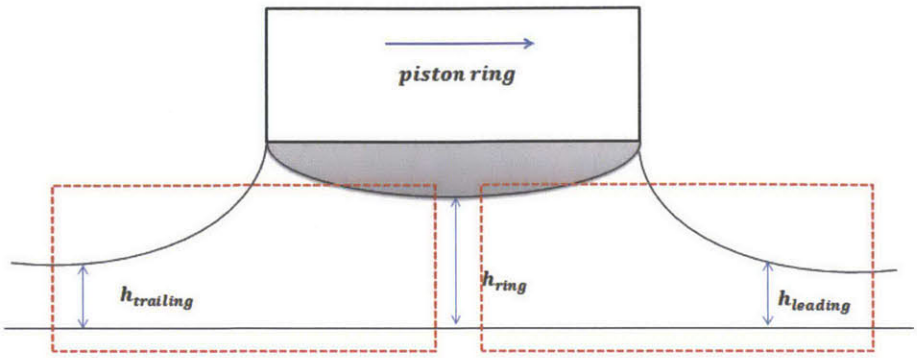

Figure 3-8: Control volumes used to solve for film thickness profiles

There is an initial oil film thickness during the intake stroke and the ring first follows this profile along the cylinder liner. After the first stroke is over, the ring reverses direction and sees the profile the ring left behind and traces a new profile as it moves along the previous profile. This process repeats for the power and exhaust stroke. This follows closely the simulation created by Tian et al [21].

3.5 Hydrodynamic Lubrication

Lubrication theory describes the flow of fluids in the situation that one dimension is significantly smaller than the others. In the case of lubricating oil on the cylinder liner, the oil film thickness h is much smaller than the length L that the oil extends to on the liner ($(h/L) \ll 1$). Different types of lubrication exists in different engine regimes. In this section, hydrodynamic lubrication and the assumptions and equations related to it are discussed.

Hydrodynamic lubrication is the support of the a surface of oil pressure along without any direct surface contact. Ring liner system under hydrodynamic lubrication involves piston velocity U and also film thickness under ring h (Figure 3-9). The liner is expected to move in the opposite direction of the piston ring movement.

By applying the conservation of mass and conservation of momentum equations, the velocity profile can be determined and then finally the volumetric flow rate can be determined. Due to the numerous variables in the conservation equations, some

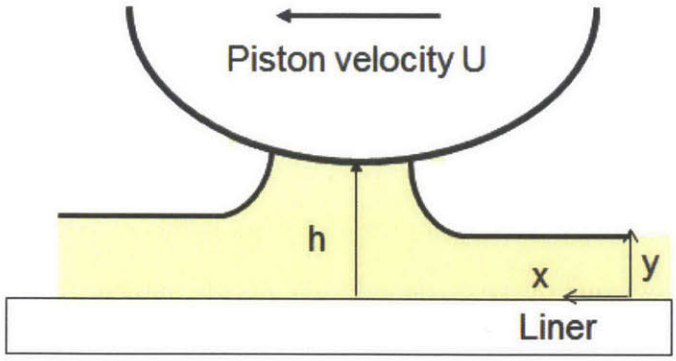

Figure 3-9: Film thickness underneath the ring at each position

simplifications are made to understand oil transport. The assumptions are as follows:

1. Laminar flow
2. No external forces act on fluid film ($X = Y = Z = 0$)
3. Height of fluid film $y \ll x$, z
4. Fluid inertia is small compared to viscous shear
5. All velocity gradients are negligible compared to du/dy
6. Negligible pressure variation across fluid film ($dp/dy = 0$)

For an incompressible, Newtonian fluid, the equations of laminar flow continuity (Equation 3.3) and momentum transport (Equation 3.4) in the x-direction are show below:

$$\frac{\partial u}{\partial x} + \frac{\partial y}{\partial y} + \frac{\partial z}{\partial z} = 0 \tag{3.3}$$

$$\rho(\frac{\partial v}{\partial t} + u\frac{\partial u}{\partial x} + v\frac{\partial u}{\partial x} + w\frac{\partial u}{\partial x}) = -\frac{\partial p}{\partial y} + \mu(\frac{\partial^2 u}{\partial x^2} + \frac{\partial^2 u}{\partial y^2} + \frac{\partial^2 u}{\partial z^2}) + \rho X \tag{3.4}$$

Due to assumption 4, the left hand side of the Navier Stokes equation is neglected because the shear forces dominate. Due to assumption 5, the velocity gradient du/dy dominates other velocity gradients. In addition, assumption 2, eliminates the body forces in the right hand side of the equation. As a result, the Navier Stokes equation reduces to Equation 3.5.

$$\frac{1}{\mu}\frac{\partial p}{\partial x} = \frac{\partial^2 u}{\partial^2 y} \tag{3.5}$$

In the flow region of interest, the bottom surface of the cylinder liner is stationary where $y = 0$. The top surface, where $y = h(x)$, there is a velocity component of piston velocity U. The lubricant adheres to the bounding surfaces and the boundary conditions are $u(y = 0) = 0$ and $u(y = h) = U$. After some simplification and using the boundary conditions, integration of the x momentum transport equation across the oil film (y-direction) derives the velocity profile shown in Equation 3.6.

$$u(y) = \frac{1}{\mu}\frac{\partial p}{\partial x}(y^2 - yh) + \frac{y}{h}U \tag{3.6}$$

As can be seen in the fluid velocity equation, there is a superposition of two distinct effects. The fluid moves due to an imposed pressure gradient called the Poiseuille flow and flows by a shear driven effect induced by the motion of the top surface called the Couette flow. The Poiseulle flow brings a parabolic velocity distribution across the film, while the Couette flow results in a linear velocity profile.

Flow rate which is derived from the velocity profile is shown in Equation 3.8, where Q is the flow rate, h is the film thickness, $u(y)$ is the fluid speed, and y is the vertical direction.

$$Q(x) = \int_0^h u(y)dy \tag{3.7}$$

After integrating $Q(x)$, the flow rate equation is derived in Equation 3.8. The mass flow rate can then be derived by multiplying the flow rate value by density ρ.

$$Q(x) = -\frac{1}{12}\frac{h^3}{\mu}\frac{\partial p}{\partial x} + \frac{Uh}{2} \tag{3.8}$$

The pressure distribution can be calculated by applying the conservation of momentum equations to a fluid element under the top ring. By using appropriate boundary conditions and assuming that the oil is incompressible, the system reduces to the $2D$ Reynold's Equation (3.9), where p is the pressure, h is the oil film thickness, U is the piston speed, and μ is the viscosity [21].

$$\frac{\partial}{\partial x}(\frac{h^3}{\mu}\frac{\partial p}{\partial x}) = 6U\frac{\partial h}{\partial x} + 12\frac{\partial h}{\partial t} \tag{3.9}$$

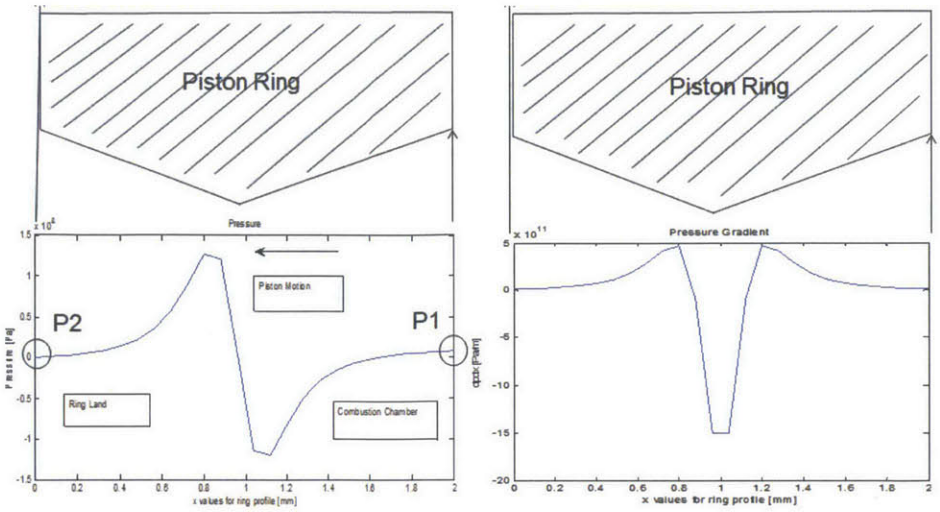

Figure 3-10: Pressure and pressure gradient for crank angle 375 degrees shows varying pressures across the piston ring and different profiles for each crank angle

At each crank angle there exists a pressure on the combustion chamber side called $P2$ and a pressure on the crankcase side called $P1$. These are the known boundary conditions for pressure distribution. After simplifications and integration, the pressure gradient and pressure equations are derived as follows:

$$\frac{\partial p}{\partial x} = \frac{6\mu U_P}{h^2} + \frac{C_1}{h^3} \tag{3.10}$$

$$P = 6\mu U_p \int \frac{dx}{h^2} + C_1 \int \frac{dx}{h^3} + C_2 \tag{3.11}$$

where $\frac{\partial p}{\partial x}$ is the pressure gradient, μ is the oil viscosity, U_P is the piston velocity, h is the ring profile equation that is a function of location.

The ring profile equation is determined by taking the top ring profile and obtaining a parabolic equation (Equation 3.12) where h is the height at a certain x coordinate and h_0 is the height underneath the ring or the minimum film thickness.

$$h = 8.284(x - 0.001)^2 + h_0 \tag{3.12}$$

The pressure distribution and pressure gradient varies along the piston ring and the profile is different for each time during the cycle (Figure 3-10).

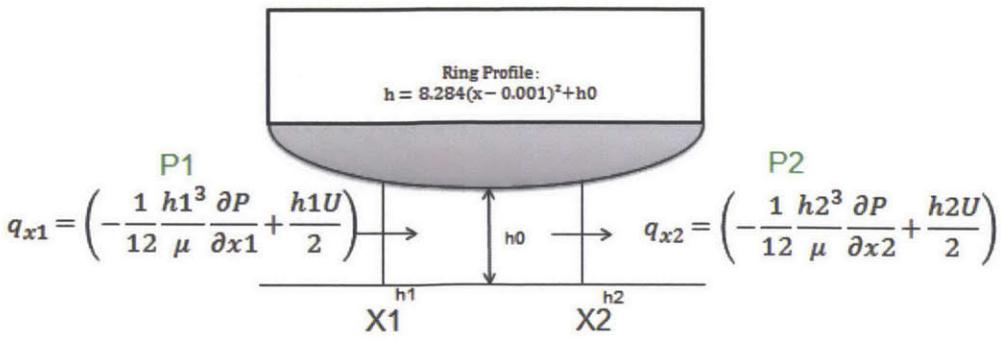

Figure 3-11: Flow rate equations underneath the ring shows the impact of pressure gradient, heights at each position, and ring profile on the amount of mass flux at each boundary

3.6 Flow Rates

Using the minimum film thickness and pressure gradient values, flow rates at every point under the piston top ring is calculated (Figure 3-11). The flow rates are shown at points $X1$ and $X2$ and also the point right underneath the ring which uses the $h0$ term. For points $X1$ and $X2$, the terms $h1$ and $h2$ are used respectively, which are calculated from using the ring profile equation discussed earlier (Equation 3.12).

The velocity curves and flow rate curves for each zone on the cylinder liner is plotted out. The velocity profile and flow rate profile for each zone is different because the piston ring passes each zone at different times during the engine cycle. For instance, if zone 4 is analyzed, initially, the velocity and flow rate is zero because the ring is not within that region of the cylinder liner and does not affect that zone. However, once the ring passes by that segment on the liner, there will be a mass flow rate and a sudden increase in flow rate in that zone. Once the ring leaves that location, it no longer affects that zone, and the velocity and flow rate is zero at that location. There are four specific "humps" of velocity spurts because the ring will pass by the zone four times in a complete engine cycle.

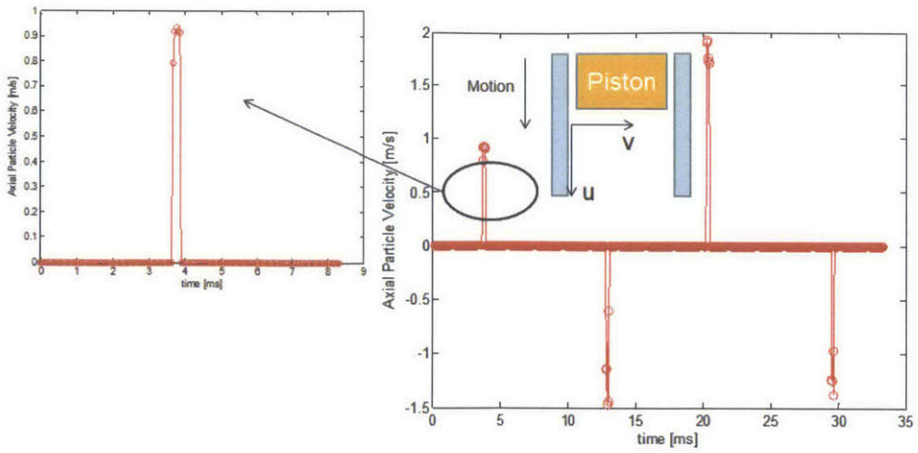

Figure 3-12: Axial velocity curve shows four changes in mass flow rates, otherwise there is zero movement

3.7 Oil Displacement

Understanding how an oil particle moves underneath the ring is important to capture oil transport. A particle in the oil layer gets dragged when the ring is near it and then stops when the ring leaves. The particle reverses direction in the next stroke (Figure 3-13). The particle is shown as a dot in the middle of the oil film. When the ring is far away, the particle is immobile, then when the ring finally passes by it, the particle moves a certain displacement and speed, then goes in the opposite direction when the ring switches directions. In terms of the speed the particle travels, the fluid that is close to the piston, or top of the oil film, moves with the piston and then the fluid on the bottom does not move at all. The fluid particle in the middle of the film layer moves slower than the piston speed.

3.8 Amount of Mass Moved/Transported

Determining how much mass is moved throughout a cycle will portray the effects of oil transport. To determine this amount, the difference in the intake and compression stroke film thickness curves are calculated (Figure 3-14). The amount of mass transported that is calculated from the area between the two curves is roughly 0.9

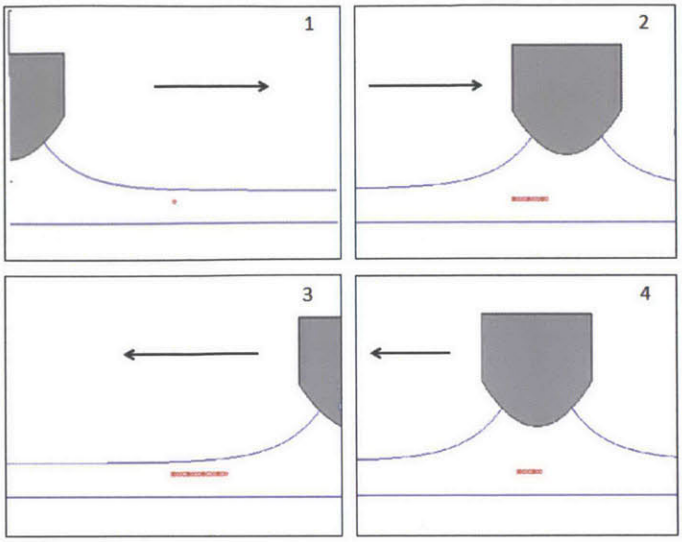

Figure 3-13: Oil displacement of a particle moves when ring drags it along oil film and stops moving when ring is no longer near it

milligrams of oil. The total amount of oil on the liner at any time is 9 milligrams. This means that the amount of mass transported is 10 % of the mass on the liner at one point. The significance of this fact is that it shows that oil is renewed every 10 cycles.

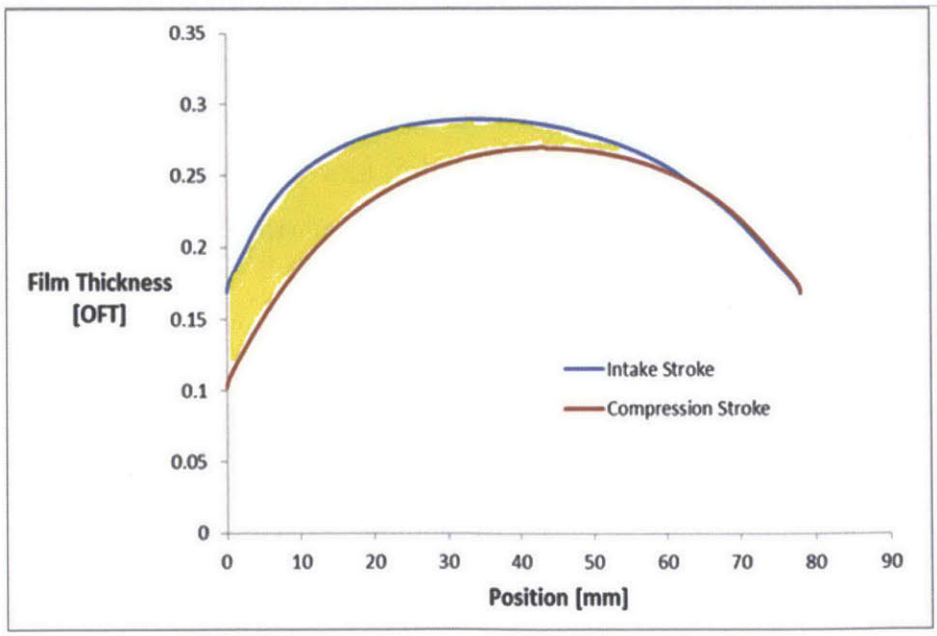

Figure 3-14: Percentage of mass moved compared to total mass in each zone for each cycle

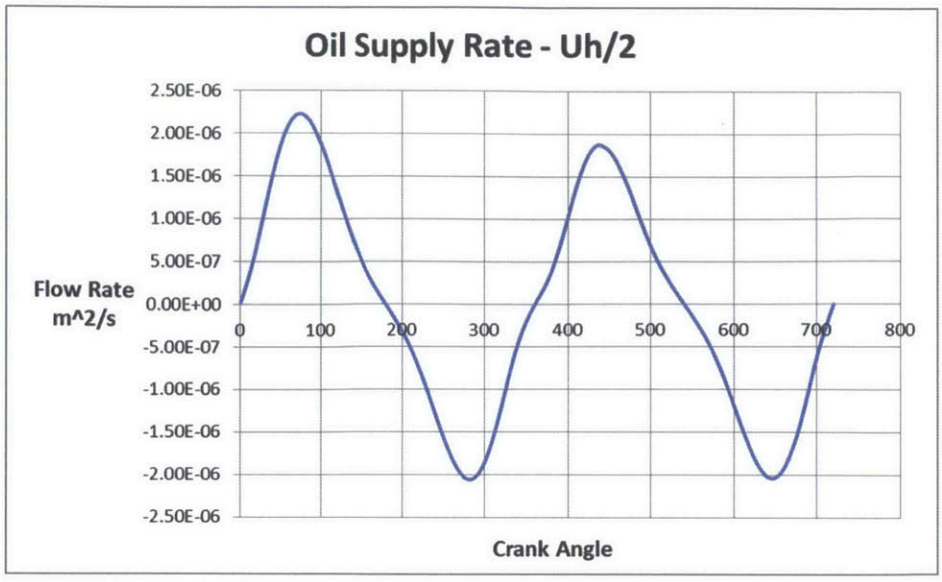

Figure 3-15: Oil supply rate calculated from flow rate underneath oil control ring

Comparing the amount of mass transported per cycle to the oil supply rate, the flow rate underneath the oil control ring is calculated. The equation for flow rate is $\frac{V \times h_{OCR}}{2}$, where V is the piston speed, and h_{OCR} is the film thickness under oil control ring. The average value for mass flow rate is 2×10^{-8} kg/s. Assuming the mass flow rate is the oil supply rate from the oil control ring to the top ring, the amount of oil transported per cycle is 1.3% of the oil supply rate. This percentage can be quite significant if summed over several hundred cycles that the engine is running.

3.8.1 Oil Composition Change Due to Mixing

Flow rates are used in the composition model in the overall equation in the incoming mass flow and outgoing mass flow portion. In the base case where there is only oil transport, there are no sources and sinks and the mathematical equation breaks down into the conservation of mass equation and composition over time can be calculated.

Chapter 4

Vaporization Modeling

In addition to composition changes due to oil transport along the cylinder liner, the oil film on the liner experiences relatively high temperature conditions which leads to significant evaporation of oil species. Vaporization of light hydrocarbon species near the top of the cylinder liner contributes to changes in composition. Studying oil vaporization is important because it is also a source of engine oil consumption. This section will discuss the modeling technique for vaporization which involves obtaining the properties of individual oil species such as vapor pressures, molecular weights, and boiling points. Mass convection coefficients are also needed to determine the vaporization rate of each species in each segment of the cylinder liner oil.

4.1 Properties of Oil Species

Volatility is an important concept when it comes to understanding the vaporization process. The more volatile the species is, the more likely it is to vaporize and leave the system. As a result, vaporization rates of different species can be used as a determining factor of its volatility. In general, the more volatile the species is, the higher its vaporization rate at a certain engine running time. Vaporization rate is used in the composition modeling equation as a sink term discussed in chapter 2. To determine vaporization rate of different species, properties such as vapor pressure, molecular weight, binary coefficients, mass transfer coefficient, and liner temperatures

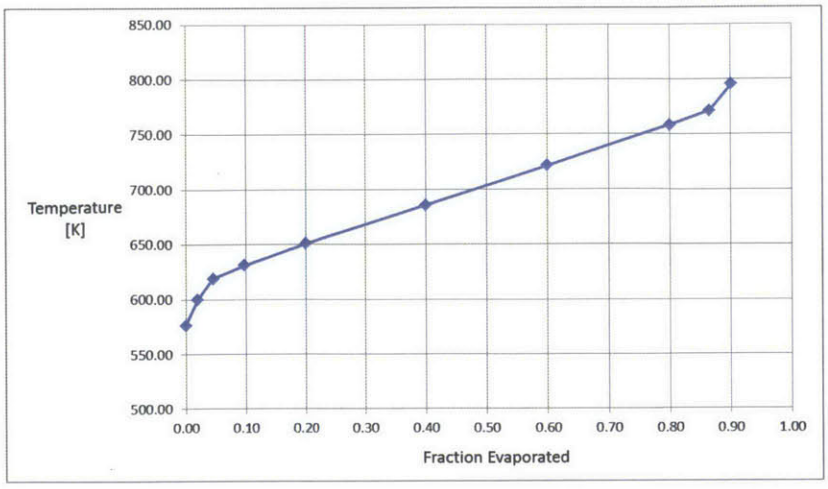

Figure 4-1: Distillation Curve shows a spread of 580K to 820K for boiling points for 15W40

are needed. These different components are discussed briefly and then ultimately combined to calculate the vaporization rate for individual species.

4.1.1 Distillation Curve

In order to determine the liquid-phase mass fraction and boiling point of each of the oil components used in this study, the distillation curve of a particular engine oil was used. Audette [3] used a span of 13 paraffin hydrocarbon components shown in a distillation curve (Figure 4-1).

4.1.2 Molecular Weight Calculation

The molecular weight of paraffin hydrocarbons can be found in Equation 4.1 by using the boiling point of each individual species. In general the heavier the species is, or the higher its molecular weight, the lower its volatility. For instance, the molecular weight of decane (C_{10}) is higher than that of nonane (C_9) and is therefore less volatile.

$$M_{oil} = a \cdot BP^4 + b \cdot BP^4 + c \cdot BP^4 + d \cdot BP^4 + e \tag{4.1}$$

where M_{oil} is the molecular weight of an oil component, BP is the boiling point of an oil component, $a = 6.072 \times 10^{-8}$, $b = -1.014 \times 10^{-4}$, $c = 0.691$, $d = -19.315$, and

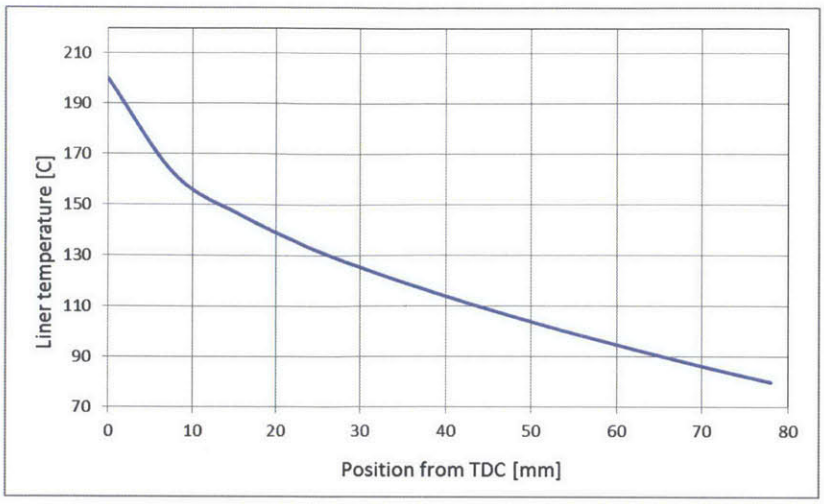

Figure 4-2: Liner temperature variation on cylinder liner with highest temperature at TDC (200°C) and lowest temperature at BDC (80°C)

$e = 2139.9082$. This correlation matches well for the paraffin hydrocarbon species C_{16} to C_{100} [17].

4.1.3 Liner Temperatures

To begin calculating vaporization rate, several gas properties are needed which depend on liner temperatures. The temperature distribution on the liner is based on the square root of the distance from the TDC of the top ring and is expressed below:

$$T_{liner} = T_{TDC} - (T_{TDC} - T_{BDC})\sqrt{\frac{y}{s}} \tag{4.2}$$

where T_{liner} is the local liner temperature, T_{TDC} and T_{BDC} are the liner temperatures at the locations of the top ring at TDC and BCD, y is the liner location relative to the TDC location of the top ring, and s is the engine stroke. Temperature varies along the liner and the BDC temperature is assumed to be 80°C and the TDC temp is assumed to be 200°C (Figure 4-2).

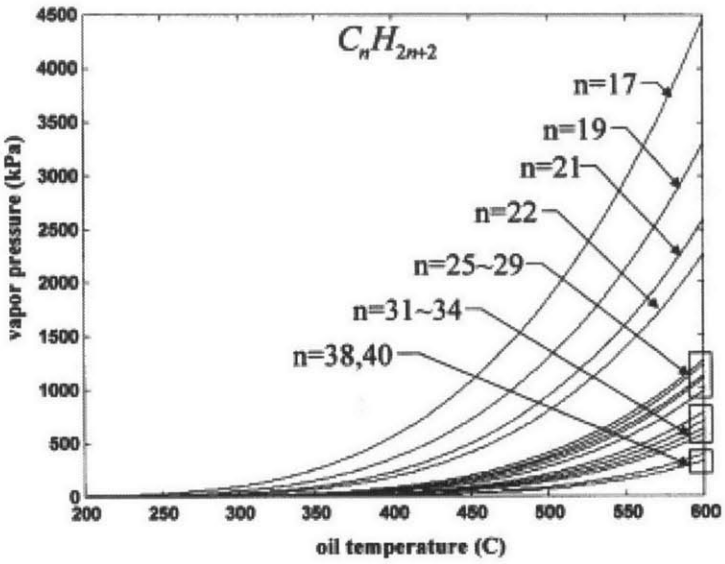

Figure 4-3: Curve of vapor pressures of oil components as a function of oil temperatures shows higher vapor pressure for higher carbon number [5]

4.1.4 Vapor Pressure of Oil Components

Vapor pressure is calculated using Antoine Equation shown in Equation 4.3. The vapor pressure of selected alkanes are calculated using this equation (Figure 4-3). This equation correlates the temperature of a paraffin hydrocarbon oil component and the vapor pressure of that component [17].

$$\log_{10}[P_{vapor}] = A - \frac{B}{C + T_{oil}} \tag{4.3}$$

where P_{vapor} is the vapor pressure of an oil component on the oil film, T_{oil} is the oil film temperature. The Antoine constants A, B, and C are tabulated by the molecular weight of different paraffin hydrocarbons.

For a given oil film temperature, a light oil component exhibits a higher vapor pressure than a heavy oil component. This highlights the fact that light hydrocarbons have the higher tendency to deplete, contributing to higher vaporization rate, and thus higher oil consumption.

4.1.5 Binary Diffusion Coefficient

The diffusion coefficient is a physical constant dependent on molecule size and other properties of the diffusing substance as well as on temperature and pressure. Different formulas exist for binary diffusion coefficients that are based on experimental investigations and empirical values. The binary diffusion coefficients for each oil species are estimated using the Wilke-Lee relation:

$$D_{12} = (0.00217 - 0.005)\sqrt{\frac{M_1 + M_2}{M_1 M_2}}\frac{T\sqrt{T}}{P}\frac{\sqrt{\frac{M_1+M_2}{M_1 M_2}}}{\sigma_{12}^2 \Omega_D} \tag{4.4}$$

where D_{12} = binary diffusion coefficient (cm^2/s), M is the molecular weight (kg/kmol), T the temperature of air oil vapor mixture in Kelvin, P is the pressure of the mixture in atm, σ the characteristic Lennard-Jones length, ω_D is the diffusion collision integral.

For a pure oil component, the Lennard-Jones length is defined as $\sigma_{oil} = 1.18V_b^{1/3}$. V_b is the Le Bas Volume and can be calculated as V_b = 14.8× (Number of Carbon elements)+3.7× (Number of Hydrogen elements). For air, σ_{air} = 3.711. For the air-oil vapor mixture, the Lennard-Jones length becomes $\sigma_{air,oil} = \frac{\sigma_{air}+\sigma_{oil}}{2}$

The diffusion collision integral is

$$\Omega_D = \frac{A}{T^{*B}} + \frac{C}{e^{DT^*}} + \frac{E}{T^{FT^*}} + \frac{G}{e^{HT^*}} \tag{4.5}$$

where A = 1.0603, B = 0.15610, C = 0.19300, D = 0.47635, E = 1.03587, F = 1.52966, G = 1.76474, H = 3.89411, and

$$T^* = \frac{T}{(\epsilon/k)_{1,2}} \tag{4.6}$$

where $(\epsilon/k)_{air,oil} = \sqrt{78.6 * 1.15T_b}$, T_b being the boiling temperature of the species. As can be seen in these complex equations, a lot of species component values are needed to be known and therefore was discussed in earlier sections.

4.1.6 Mass Transfer Coefficient

Low Mass Transfer Assumption

Low mass transfer assumption involves the biot number, which is defined as the ratio of the oil species diffusion resistance in the liquid to the convection resistance in the gas phase. The equation is shown below:

$$Bi = \frac{h_m L_C}{D_{AB}} \tag{4.7}$$

where Bi is the Biot number, h_m is the film mass transfer coefficient, L_C is the characteristic length and D_{AB} is the mass diffusivity. A small biot number indicates that the diffusion resistance is negligible and oil evaporation is limited by gas side convection. Doing a rough approxination, h_m is on the order of 1×10^{-3}, L_C which is the length of film thickness is on the order of 1×10^{-6}, and D_{AB} is on order of 10×10^{-6} gives us the value of biot number approximately 1×10^{-4} which is small, meaning we can use low mass transfer assumption.

Mass and Heat Transfer Analogy

Using the analogy between heat and mass transfer, a low mass transfer rate convection process is assumed. The equations for mass and heat transfer analogies are:

$$\begin{aligned} Sh &= 0.035 \cdot (Re)^{0.7} \times (Sc)^{0.667} \\ Re &= VL/\nu \\ Sc &= \nu/D_{ab} \\ g_m &= (Sh \cdot (\rho \cdot D_{ab}))/L \end{aligned} \tag{4.8}$$

where Sh is the Sherwood number, Re is the Reynolds number, Sc is the Schmidt number, V is the velocity, L is the characteristic length, ν is the kinematic viscosity, D_{AB} is the diffusivity, ρ is the density, and g_m is the mass convection coefficient. These are the correlations used to ultimately solve for g_m, the mass convection coefficient [3].

4.1.7 Vaporization Rate Calculation

Oil properties can now be applied to the overall vaporization rate equation shown below:

$$\dot{m}_i = g_i \cdot (mf_i - mf_\infty) \tag{4.9}$$

where g_i is the mass convection coefficient for a particular oil species, mf_i is the mass fraction of oil vapor at the cylinder surface for that species, and mf_∞ is the mass fraction of that species in the bulk cylinder gasses. Due to the large mass of cylinder gasses relative to the small mass of expected oil vapor, mf_∞ is assumed to be zero. The vapor mass fraction at the oil film surface is computed from the local vapor pressure of the oil species of interest shown below [5]:

$$mf_i = (\frac{mf_{l,i} \cdot P_{v,i}}{P_{cyl}})(\frac{MW_i}{MW_\infty}) \tag{4.10}$$

where $mf_{l,i}$ is the local instantaneous mole fraction of the species in the liquid oil film, $P_{v,i}$ is the vapor pressure of the oil species at the local instantaneous temperature of the surface of the oil film, P_{cyl} is the instantaneous pressure of the bulk cylinder gas, MW_i is the molecular weight of the oil species, and MW_∞ is the average molecular weight of the gas in the wall boundary layer. Since the total molar fraction of the oil species in the boundary layer gas is low, MW is taken to be the molecular weight of air, which is 28 g/mol.

4.2 Composition Changes Due to Vaporization

The vaporization rate during the engine operation changes as long as the mf_i, which is the local instantaneous mole fraction of the species in the liquid oil film, changes. This composition of the oil species is constantly being updated after each time step during the model. Vaporization is now used as a sink term in the overall equation that also includes incoming mass flow and outgoing mass flow. A first order differential equation is solved every time step and composition is obtained. Applications for this change in composition will be discussed in the next chapter.

Chapter 5

Rheology Application

Now that oil transport and vaporization concepts were discussed in the previous two chapters, specific applications can now be investigated. An important fact to remember about oil composition is that it is not a static parameter of a lubricant. Oil composition changes with time and space. This chapter will discuss the different factors that cause oil composition to not be a static parameter. Chapter 1 briefly discussed these processes and a summary of the chemical and physical processes that change oil composition along the cylinder liner are:

- Fuel impingement
- Oxidation/degradation of oil
- Combustion gas contamination
- Vaporization
- Piston Movement
- Soot contamination

Composition changes due to the above processes affect oil rheological properties. This chapter will focus on introducing blending equations with vaporization and oil transport processes (Figure 5-1). It will begin by discussing the importance of studying changes in oil rheology then discuss the effects of temperature and vaporization on viscosity.

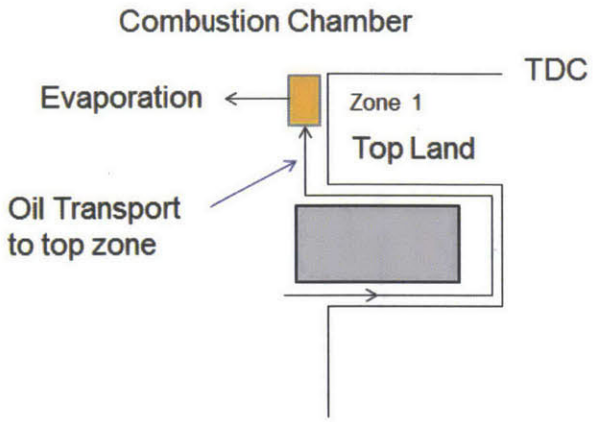

Figure 5-1: Schematic of oil transport and vaporization effects on cylinder liner oil

5.1 Oil Rheology

Changes in composition of oil causes changes in its viscosity. A change in viscosity causes a change in friction and understanding changes in friction can help oil formulators understand how to optimize the lubricant for increased engine efficiency. This section introduces the importance of studying viscosity with the Stribeck curve. It will be noted from the Stribeck curve that the oil viscosity has a major impact on the friction coefficient, and therefore its engine efficiency.

5.1.1 Stribeck Curve

The lubrication regime is determined by the fluid viscosity, the load that is carried by the two surfaces, and the speed that the two surfaces move relative to each other combine to determine the thickness of the fluid film. The various modes of lubrication includes hydrodynamic, boundary, and mixed lubrication. Changes in sliding speed, load, and oil viscosity affect each mode differently.

In order to understand the relative contributions of each regime, the Stribeck curve (Figure 5-2) was developed to illustrate the distribution of hydrodynamic, boundary, and mixed lubrication for various speeds. The Stribeck curve plots friction as it relates to viscosity, speed, and load. The vertical axis is the friction coefficient and

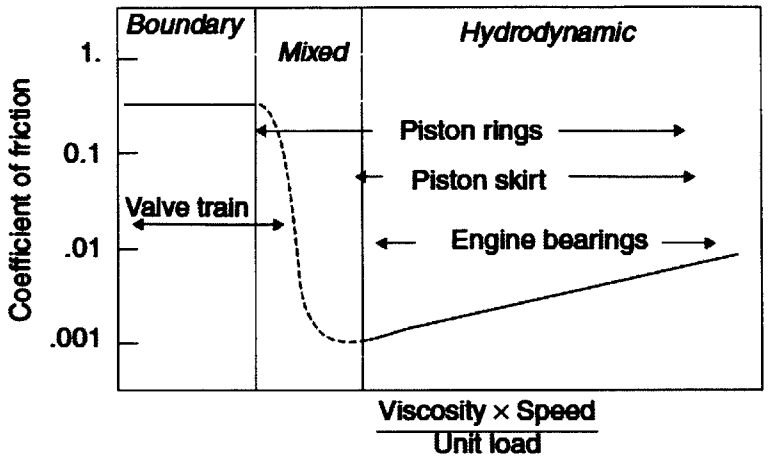

Figure 5-2: Stribeck Curve shows three lubrication regimes: boundary, mixed, and hydrodynamic modes [15]

the horizontal axis shows a parameter that combines the other variables fluid viscosity, the relative speed of the surfaces, and the loading force per unit area [10][15].

The combination of low speed, low viscosity, and high load will produce boundary lubrication which is the regime where there is little fluid in the interface and there exists large surface contact. This is the location of high friction. When the speed and viscosity increases or if the load decreases, the surfaces will begin to separate and a fluid film begins to form. The film is thin but acts to support more of the load, which results in mixed lubrication. The decrease in friction coefficient is a result of decreasing surface contact and more fluid lubrication.

As the surfaces separate as the speed or viscosity increases, a full fluid film will appear. The friction coefficient will reach its minimum where it transitions to hydrodynamic lubrication. This is the regime where the load on the interface is entirely supported by the fluid film. There is low friction and no wear in hydrodynamic lubrication since there is a full fluid film and no solid to solid contact. The friction increases in the hydrodynamic region. This is due to fluid drag which is friction produced by the fluid. The higher speed may result in thicker fluid film, but it also increases the fluid drag on the moving surfaces. A higher viscosity will increase the fluid film thickness but at the same time increase the viscous drag [10].

5.1.2 Significance of Viscosity Parameter

The Stribeck curve informs design decisions by suggesting the direction in which to change various parameters. The ideal lubrication condition occurs when net friction is minimized which is at the lowest point on the solid curve. As seen from the plot, friction is minimized when the piston is supported by a combination of boundary and hydrodynamic lubrication, which is known as the mixed lubrication. In general, if there is hydrodynamic friction, the oil viscosity can be decreased to minimize friction. However, if boundary friction predominates, increasing oil viscosity can actually decrease friction by moving lubrication toward the right on the curve. Generally, the speed is fixed by engine speed and geometry, and loading force per unit area is fixed by cylinder pressure and connecting-rod geometry. Consequently, viscosity seems to be the only significant parameter in the Stribeck curve that can be modified. As a result, studying viscosity changes in the engine is very important and can be used as a mechanism to control friction coefficient in the engine.

5.2 Temperature Effects on Viscosity

Viscosity of oil species depend on several factors and one of them includes temperature. Different species have different temperature versus viscosity curves and numerous research papers discuss ways to calculate the viscosity μ as function of temperature. The most widely used correlation is the Andrade equation [13]:

$$\ln(\mu) = A + \frac{B}{T} \tag{5.1}$$

where A and B are parameters and T is temperature. This equation can be used successfully for interpolating experimental viscosity data and extrapolation up to approximately the normal boiling point for light boiling components. Modifications of the Andrade equation have been proposed to improve its accuracy, such as the Vogel equation:

$$\ln(\mu) = A + \frac{B}{T + C} \tag{5.2}$$

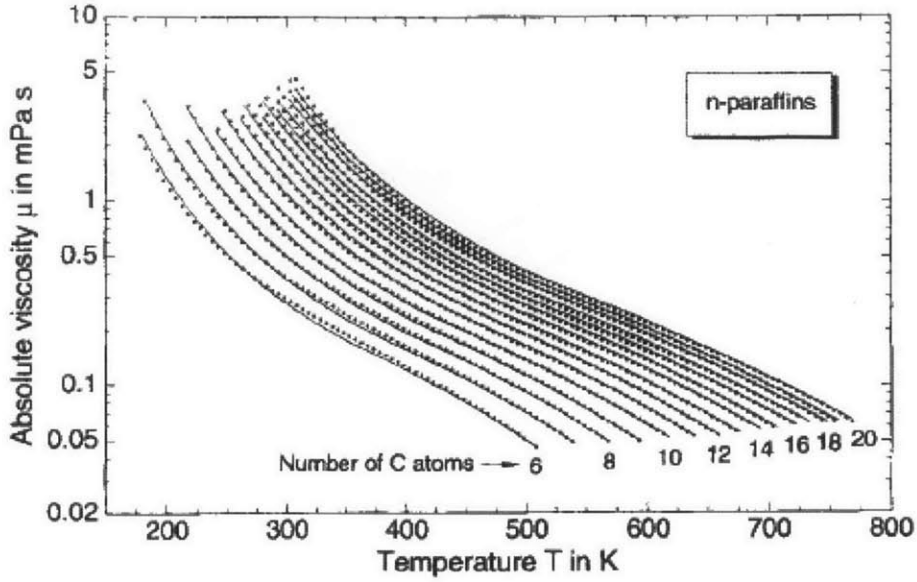

Figure 5-3: Experimental viscosity data of n-paraffins shows decreasing viscosity with increasing temperature [13]

This equation has pretty much the same variables as the Andrade equation, but, as can be seen in the Vogel equation, there is an extra third parameter C. In addition to the equations shown above, there are also experimental viscosity data of paraffins (Figure 5-3). Walther's formula, which is the formula used in the authors work is shown below:

$$\log\log(\nu + 0.7) = A + B\log T \tag{5.3}$$

where A and B are determined from knowing the viscosities of the different species at 40°C and 100°C. The use of the Walther's equation for two different grades of oil are shown in Figure 5-4. As a conclusion, it can be seen there as temperature increases, viscosity of the oil species decreases.

5.3 Introduction to Blending Equations

After mixing, different oil components with different composition and different viscosity temperature relationships exists in each individual zone. The zones being the

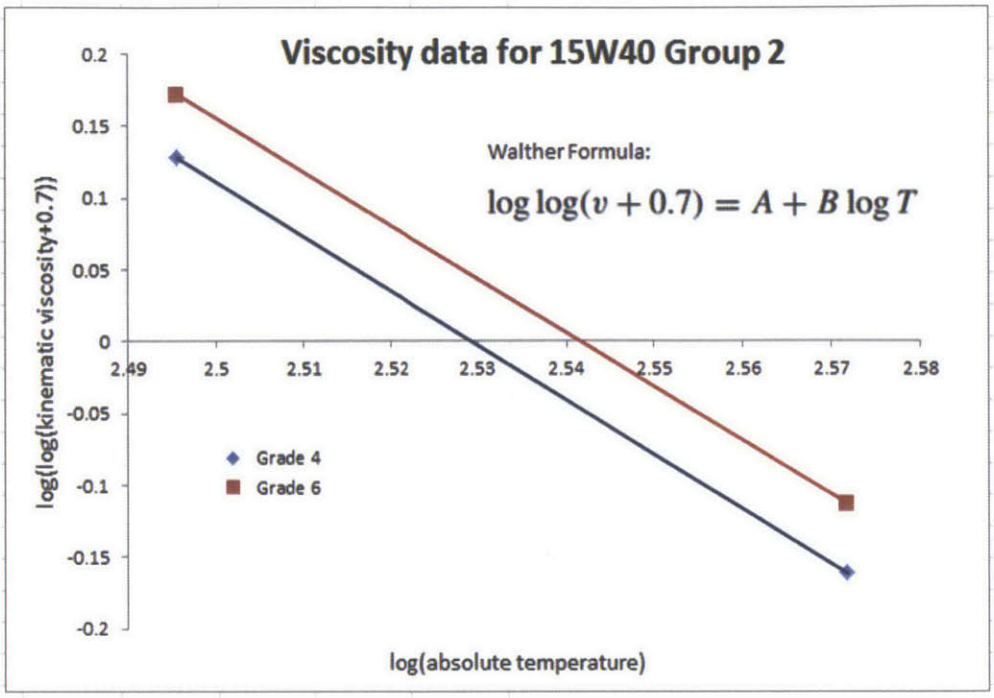

Figure 5-4: Viscosity curve for two different grades of oil using the Walther's formula

individual segments divided on the liner discussed in previous chapter. Each zone has a different composition and to go from composition to viscosity there needs to be a link that would be coming from a blending equation. This section will discuss the method of calculating a mixture from pure component viscosity weighted by their composition to eventually see the effects of vaporization on oil viscosity.

5.3.1 Composition Values

Different engine inputs and different oil species with oil transport and vaporization processes occuring on the liner cause composition changes with position and time. Composition can then be used in different mixing equations. There are many correlations that mix different species, including hydrocarbons. Composition for each species also varies in different zones for each species. For instance, composition of a hydrocarbon species $C_{10}H_{22}$ in the first segment along the liner is different from the composition of the same species in the second segment due to its higher volatility near the top of the cylinder liner.

5.3.2 Types of Blending Equations

Blending equations are widely used in industry. Many companies have blending models in which when they input a certain composition of base oils and viscosity modifiers, it would output a overall viscosity curve for the mixture. Trying to apply something similar to that, many blending equations are looked at and discussed in this subsection [20].

Arrhenius Equation

One equation that has been used to model alkanes is the Arrhenius equation (Equation 5.4). After obtaining composition at each position along the cylinder liner, the mixture viscosity can be determined. This equation has been known to be used widely and quite accurate.

$$\ln(\mu_{mixture}) = \sum_{i=1}^{n} X_i \ln(\mu_i) \tag{5.4}$$

where $\mu_{mixture}$ is the overall viscosity of the mixture, n is the number of species components in the mixture, X_i is the mass fraction of the individual component, and μ_i is the component viscosity.

Kendall and Monroe

Another widely used blending equation slightly different from Arrehenius is the kendall and monroe shown below. As can be seen the variables are the same as Arrhenius and the differences lie in the exponents and logarithms.

$$\mu_{mixture} = (\sum_{i=1}^{n} X_i(\mu_i)^{1/3})^3 \tag{5.5}$$

Bingham

The last method that this subsection will show is the Bingham method that instead of using X_i which is the mass fraction in the previous equations, it uses V_i which is the volume fraction, which shows a slight difference from the other equations.

$$(\mu_{mixture})^{-1} = \sum_{i=1}^{n} V_i(\mu_i)^{-1} \tag{5.6}$$

5.4 Determination of Viscosity Temperature Curves

Looking at the blending equation, the viscosity temperature of each species needs to be determined along with the composition. In general, the degree of compositional information decreases with increasing boiling range. Gas or light fractions can be completely analyzed. For heavier fractions, exact information about type and position of branches at paraffinic structures or paraffinic side chains on ring molecules is not available. As can be seen in the oil species properties, the boiling points of those species are quite high.

5.4.1 Kinetic Gas Theory

The kinetic gas theory represents a fundamental tool for predicting gas viscosity. The mobility in gases is primarily determined by the molecules in free flight, ideally without interactions, and so is viscosity. In the liquid phase, molecules travel only short distances, and interactions between colliding molecules play the most important role. These interactions are determined by the structure of the molecules and by the degree of disorder within the arrangement. Statistical mechanics represents a fundamental idea about the interactions of molecules in liquids. However, in order to be able to predict properties like viscosity, proper distribution, functions describing the intermolecular force field or the intermolecular potential energy functon are needed. These distribution functions in the Lennard-Jones potential function require information about a characteristic collision diameter. For liquids, this is okay to determine, but solids in the high C numbers, these properties are not found [10].

5.4.2 Heavier Alkanes are Solids

Alkanes can be split into gas state, liquid state, and solid state. Specifically, carbon numbers $C_1 - C_4$ are in the gas phase at room temperature, $C_5 - C_{15}$ are in the liquid phase, $C_{16} - C_{18}$ are in the semi-solid wax state, $C_{20} - C_{40}$ are solid waxes, and C_{40} onwards are solid ashpaltines. In general any carbon number higher than 16 are solids. Oil packages ranges in carbon numbers all the way to C_{60}, explaining the difficulty to get component viscosities at specific temperatures.

5.4.3 Extrapolation of Data

The method employed in this study to handle the higher alkanes is using the lighter species component viscosity curve and extrapolating from it. For instance, all the lighter hydrocarbons have a viscosity curve similar to the one shown in Figure 5-3. Specific parameters of the temperature dependence of the lighter hydrocarbons using the Walther's equation were estimated using best judgment. The higher hydrocarbons are just assumed to all line higher than those n-paraffin curves. This is the assumption used and will give results in the right magnitude.

5.5 Model Inputs

Engine specifications are still the same as the Kohler engine discussed in Chapter 2. Oil specifications are discussed in this section.

5.5.1 Oil Specifications

The oil package that was used for this application is a typical 15W40 with the molecular weights and boiling points of the individual species shown in Figure 5-5. In this package, only alkane or paraffins were used because of its widely known properties. The chemical formula of these alkanes are C_nH_{2n+2}, where n is the carbon number of the species. Alkanes consist only of hydrogen and carbon atoms, all bonds are single bonds.

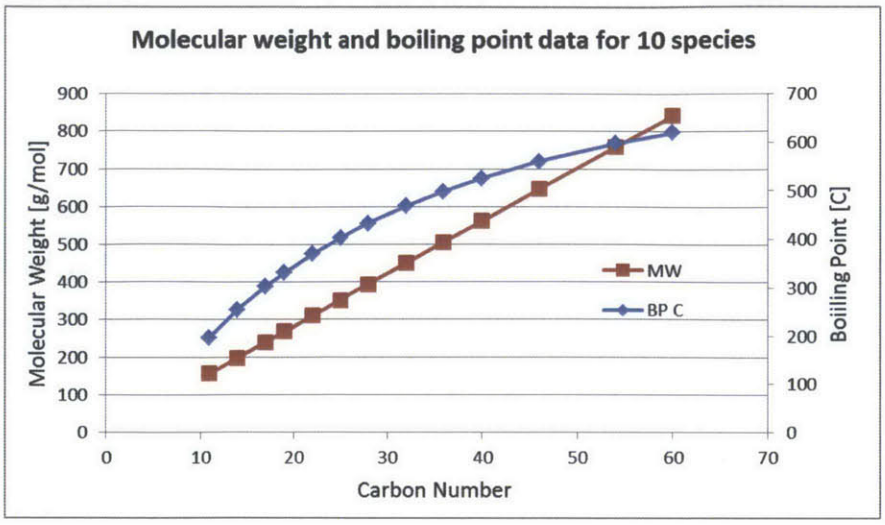

Figure 5-5: Oil species boiling point and molecular weight

5.6 Results on Viscosity Variations

Since viscosity is related to friction in many ways shown in the Stribeck curve, studying what changes viscosity is important. This section will results of the composition model that portrays the effects of temperature and vaporization on viscosity.

5.6.1 Temperature Effects

Discussed earlier in this section is the temperature effects on oil viscosity. At higher temperatures, viscosity is lower and at lower temperatures, viscosity is higher. Viscosity modifiers are used to decrease the sensitivity of oils to these temperature effects. The temperature effects on oil viscosity and the magnitude of difference in temperature at top dead center and bottom dead center is discussed in the first chapter.

5.6.2 Vaporization Effects

Vaporization effects on oil viscosity is due to the volatility of the oil species. High temperatures in the combustion chamber causes light species vaporize and leave the heavier species with higher molecular weight behind near the top dead center zones. These heavier molecules have higher viscosity at that location and there its composi-

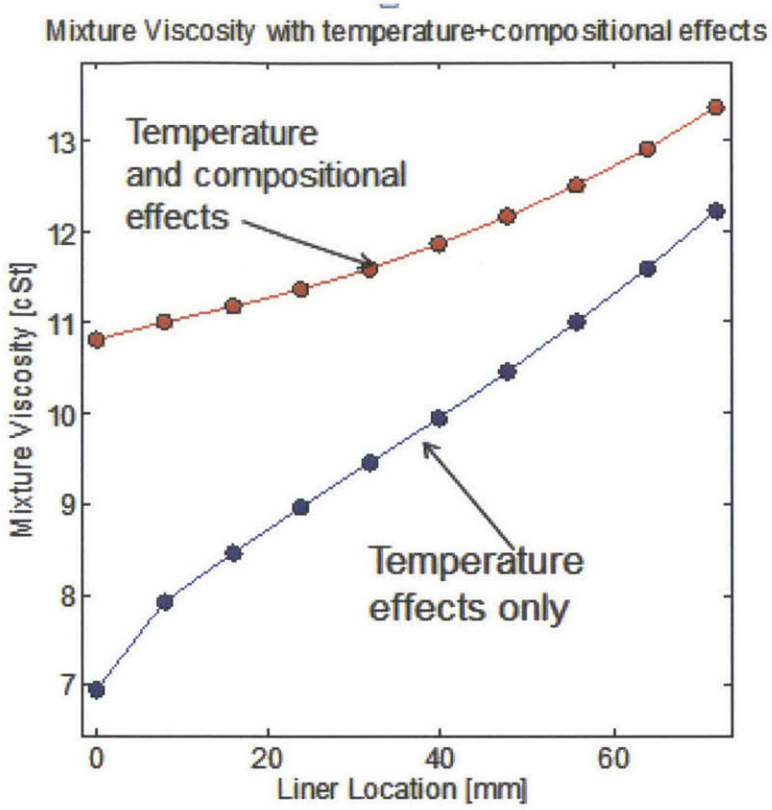

Figure 5-6: Vaporization effects on oil rheology shows higher viscosity near the top dead center than with only considering temperature effects

tion is also higher. The heavier molecules contribute more to the zone's composition and therefore increase the overall viscosity of the zone [16]. As a result, vaporization process is known to induce higher viscosity oil near the top of the cylinder liner.

5.6.3 Combination of Temperature and Vaporization Effects

The model attempts to simulate both the temperature and vaporization effects on viscosity. The method involves using the oil species distribution laid out in the previous section and vaporization concepts from Chapter 2. Vapor pressure, binary coefficient, mass transfer coefficient, and vaporization rates were solved for each species. Then the general composition modeling equation is applied to solve for the composition over time and space. After obtaining composition at each position along the cylinder liner, the mixture viscosity is determined from the Arrhenius Blending Equation

discussed in the section of blending equations.

Applying the Arrhenius blending equation, viscosity can be determined from composition results from vaporization shown in Figure 5-6. It can be seen that with just temperature effects, the viscosity is lower near top dead center where temperatures are higher. But due to vaporization, the lighter hydrocarbons species vaporize near the top of the cylinder and leave heavy ones behind. Heavy molecules have higher individual viscosities and makes the viscosity near top dead center greater than the light molecules would. Therefore, the curve with compositional and temperature effects is greater than the curve with only temperature effects. This idea that there would be higher viscosity near the top dead center rises the possibility of getting a flatter viscosity curve, which helps to reduce wear effects in the top of the liner. As can be seen in this chapter, vaporization affects the rheology of the oil. In reality, vaporization is only one of the many things that affect oil rheology. The next chapter will discuss other applications that builds off the two concepts of oil transport and vaporization.

Chapter 6

Other Applications

In addition to studying vaporization effects on rheology, other applications such as additive effects, fuel impingement, and soot contamination on oil rheology from compositional effects are studied. This chapter will expand on the previous chapter of modeling effects of different applications on oil rheology.

6.1 Additive Concentration Modeling

Up to this point, most of the oil species discussed are hydrocarbons, but oil packages are not only made up of base oil hydrocarbons. In addition to the base oil, additives are added to the package to protect the base oil, and it is important to understand the effects of additives on oil composition. Differences between base oil and additive properties are that base oil makes up a bigger percentage overall in the oil package and also differences lie in their volatility. Additives are on average less volatile than base oil. Important additives include ZDDP and detergents, which are made up of mainly calcium sulfate and zinc phosphate elements. Due to vaporization, light hydrocarbon species vaporize and leave the top zone areas, retaining more of the composition of the additive species.

Additive concentration retention was studied by Simon Watson, a former MIT PhD student [25]. This section will discuss Watson's experimental data setup and results. A similar process will be applied to the author's current composition model

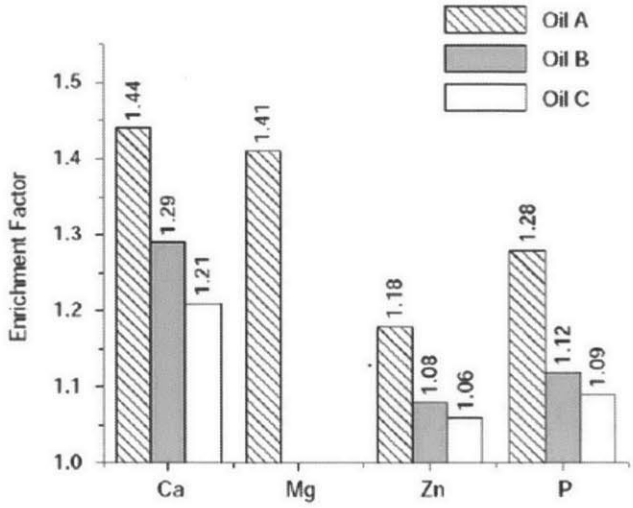

Figure 6-1: Simon Watson's experimental results for additive concentrations shows enrichment factors greater than unity for all elements [25]

and simulation results will be observed. Simon's experimental data will be compared to simulation results from composition model to have a way of validation.

6.1.1 Experimental Data of Additive Concentrations

Watson performed experimental studies on enrichment factors of different elements in different parts of the engine. Enrichment factor is designated as the concentration of the additive in the piston ring pack zone divided by the concentration of the additive in the sump. Simon did this study on lubricant composition because he wanted to understand ash emissions and additive requirements. He solved for enrichment factors (Figure 6-1) for different additive species such as Calcium, Magnesium, and Zinc in different oil sampling zones (Figure 6-2). He sampled from three main locations: sump, ring pack zone, and valve-train. Specifically when he mentions ring pack zone, it refers to the oil behind the top ring of the piston.

Watson concluded that calcium and magnesium are concentrated to the highest degree and these elements are associated with detergent additives in the lubricant. The lowest enrichment factors are found for zinc and phosphorus, which are associated with ZDDP. Watson's results is a good benchmark to use in the current composition

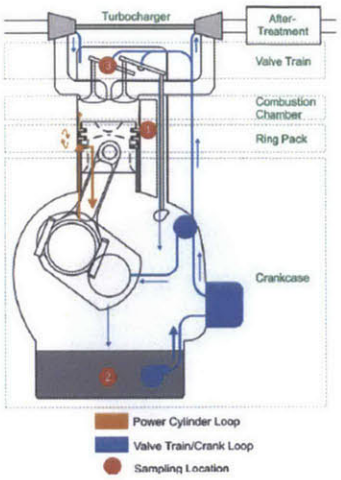

Figure 6-2: Watson's sampling regions which include ring pack zone, valvetrain, and sump [25]

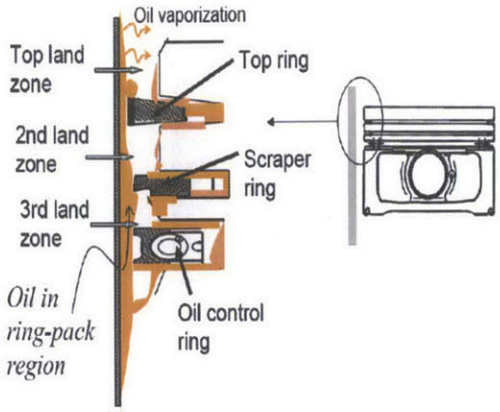

Figure 6-3: Zoom in figure on ring pack zone showing all three rings in detail [25]

to see the effects of additives on engine oil composition in cylinder liner. The next subsection will discuss the oil modeling approach for additives.

6.1.2 Modeling Approach

Similar to the base model used for vaporization and oil transport, the cylinder liner is broken up into ten zones (Figure 6-4) and each zone's composition over time is modeled. The zones schematic and oil species breakdown shows the top zone is modeled as the ring pack zone and the BDC zone is modeled as the sump zone corresponding to Simon's sump zone sampling region (Figure 6-4). These relative locations chosen on the cylinder liner oil should approximate the areas within the engine Watson chose for his experiments. The BDC zone, or last zone, should be relatively close to sump zone's concentration because less vaporization occurs in that location.

The original hydrocarbon species for the previous examples are 100% hydrocarbon, while in this approach, two additive species are also included to simulate the additive package and to determine enrichment factors. These additive species make up a lesser proportion of the oil package compared to the hydrocarbons (Figure 6-5). The goal

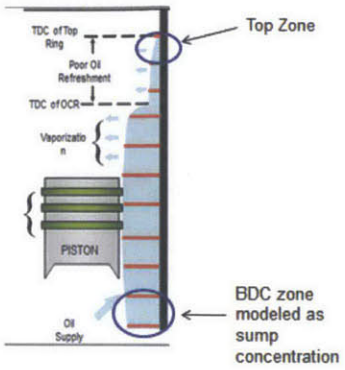

Figure 6-4: Zone modeling approach compared to Watson's sampling regions

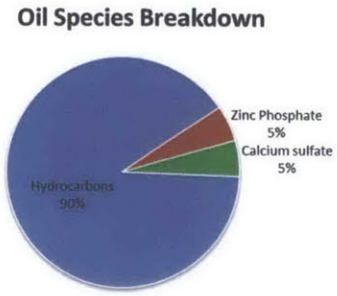

Figure 6-5: Pie Chart with species breakdown for additives+hydrocarbons

of this additive study is to compare experimental enrichment factors to simulation enrichment factor values.

6.1.3 Simulation Results

Using the modeling approach discussed above, composition results were obtained for calcium sulfate and zinc phosphate. A bar graph that compares experimental results to simulation results of enrichment factors was made (Figure 6-6). Three bar chart numbers are shown for each element. First, the very first bar is Watson's experimental data for that element. The second value is the composition model's solved for enrichment number using the very top zone as the "ring pack zone" in Watson's experimental data. This number seemed a bit high compared to experimental data and that is where the third bar came in. The third bar is using the average of the top three zones so it wouldn't just be taking the top zone, which has extremely high vaporization rates, value into account because it might not completely compare well with Watson's ring pack zone. Once an average was taken to compare with experimental results, a closer enrichment value was obtained. This shows that the sampling location cannot correspond directly to liner location.

A few things to note is that both the simulation results and the experimental

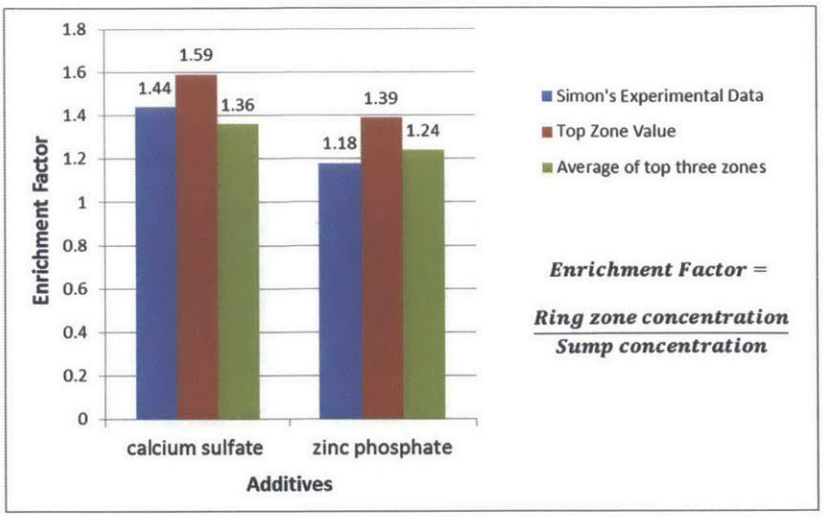

Figure 6-6: Experimental results compared to simulation results

results show enrichment factors greater than unity. This makes sense due to the vaporization of light hydrocarbon oil and therefore the retention of these additive elements. In addition, it also shows that different volatility of elements creates different enrichment factors. For instance, calcium is less volatile than zinc and therefore is more retained than the zinc phosphate in the ring pack, which is shown by the higher enrichment factor values of calcium.

6.2 Fuel Impingement on Oil Composition

Fuel impingement due to late injection is another process that affects the cylinder liner oil. This section will describe the fuel dilution modeling and validation.

6.2.1 Introduction

To meet emissions, the Diesel Particulate Filter (DPF) needs to trap soot for thermal management purposes. To avoid filter plugging, the accumulated soot needs to be burned off. A plugged filter will cause high backpressure and operational issues. Many Original Engine Manufacturers (OEMS) use a regeneration scheme in which fuel is introduced late in combustion to create an exothermic reaction downstream in the

filter, which burns off the soot. The resulting ash from regeneration of the filter can collect for thousands of miles.

6.2.2 Late Injection Effects on Fuel Dilution

The benefits of late injection is involved with its role in thermal management. But there are drawbacks with using the technique late injection because it increases the amount of lubricant exposed to the fuel. During the power stroke if injected late, the fuel spray will have a higher chance to hit the oil on the liner instead of the piston bowl. More fuel getting into the oil causes more fuel dilution. Excessive oil dilution has the potential to lead to several problems such as reducing oil performance and durability due to decreased viscosity or the development of oil sludge and catalyst poisoning.

6.2.3 Dilution Levels

Late injections of fuel can result in impingement of liquid fuel on the surfaces of the combustion chamber. Typical design for fuel in terms of oil limit dilution is 5%. Fuel dilution decreases the viscosity of the engine oil, reduces its film thickness, and decreases the concentration of oil additives. Two main mechanisms which impact dilution levels are: the rate fuel enters the oil and the rate fuel leaves the oil. Fuel enters the oil when it fails to vaporize and remains in the cylinder in liquid form. Fuel can be removed from the oil through evaporation. Rates of evaporation of fuel from oil play a critical role in determining overall dilution rates. Fuel dilution rates are depicted in Figure 6-7 for the ultra low sulfur diesel (ULSD), and is shown at many oil drain intervals [2].

6.2.4 Fuel Dilution Impact on Engine Oil Viscosity

Experimental studies have shown that viscosity decreases with fuel dilution. Viscosity decreases as mileage increases for both regular diesel and biodiesel (Figure 6-7). Biodiesel is a renewable fuel derived from vegetable oil, animal fat, or waste cooking

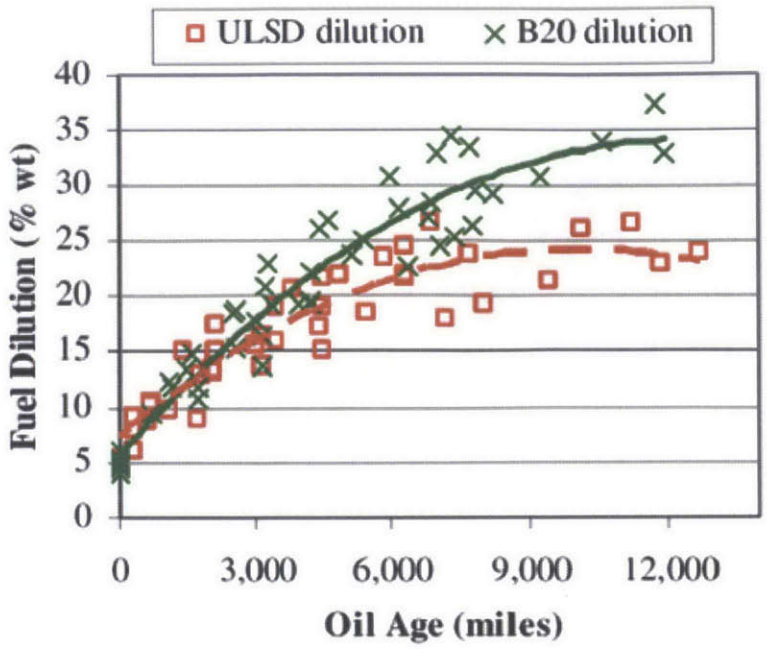

Figure 6-7: Fuel dilution percentage comparisons for biodiesel and ULSD [27]

oil and consists of methyl esters of fatty acids. It is usually used as a diesel blending component at levels up to 20% by volume. The benefits of using biodiesel lies in the fact that they release few pollutants like carbon dioxide into the atmosphere. In addition biofuels are produced from energy crops so are sustainable and if every nation grows its own, society will have an unlimited amount of biofuel. Vehicles that run on biodiesel also get 30% better fuel economy than gasoline-powered vehicles. However, biodiesel has negative influences on fuel dilution [2].

Due to the fact that a fuel with a higher vaporization rate will vaporize and not dilute the fuel, fuels with lower vaporization rates tend to stay in the oil. Biodiesel became a concern because if its higher boiling temperature. Higher concentrations of fuel are believed to accumulate in the oil with biodiesel than with petrodiesel because biodiesel has a higher boiling temperature range, allowing it to persist in the sump [27]. This leads to a concern about oil dilution for biodiesel (Figure 6-8). The figure further shows the biodiesel curve has a sharper decrease in viscosity than the ULSD curve.

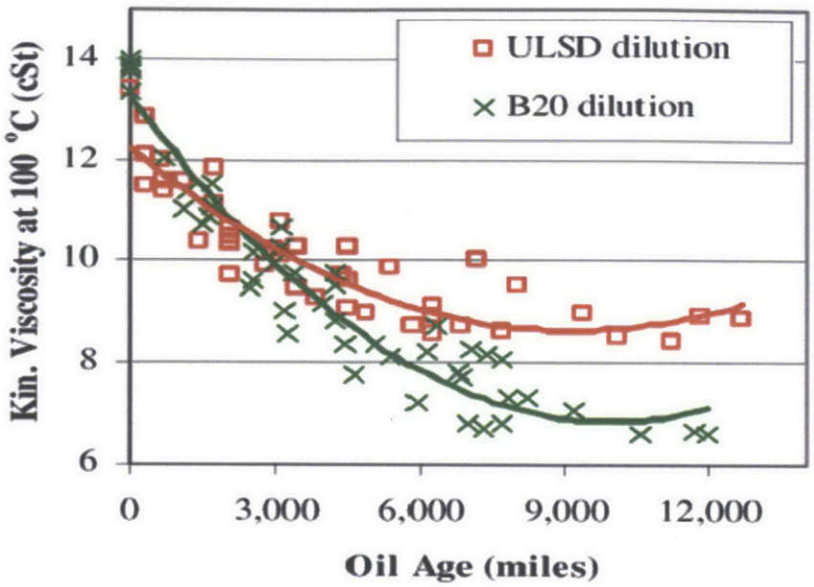

Figure 6-8: Fuel impingement effects on viscosity for biodiesel and ULSD [27]

6.2.5 Modeling Fuel Impingement Method

In previous schematics, only vaporization and oil transport was shown (Figure 5-1). Now with fuel impingement, another additional parameter needs to be added along the entire liner (Figure 6-9). This parameter of fuel impingement is not only in the first zone as it was for vaporization, but along the entire liner. Volatility of oil depends on the oil species properties in that zone while fuel impingement depends on the fuel spray and late injection.

6.2.6 Model Assumptions

For modeling purposes, it is assumed that there is a 5% fuel dilution rate, which is common for many engines designs. Some operating conditions do have fuel dilution up to 10%. It is also assumed that this 5% addition of fuel is distributed evenly across the liner in the zones. The mass of fuel added to each zone with individual fuel dilution rate is $m_{fuel} = 0.05 * (m_{fuel} + m_{oil})$. This mass of fuel is added during each power stroke of the cycle. The details of fuel impingement in terms of fuel injection

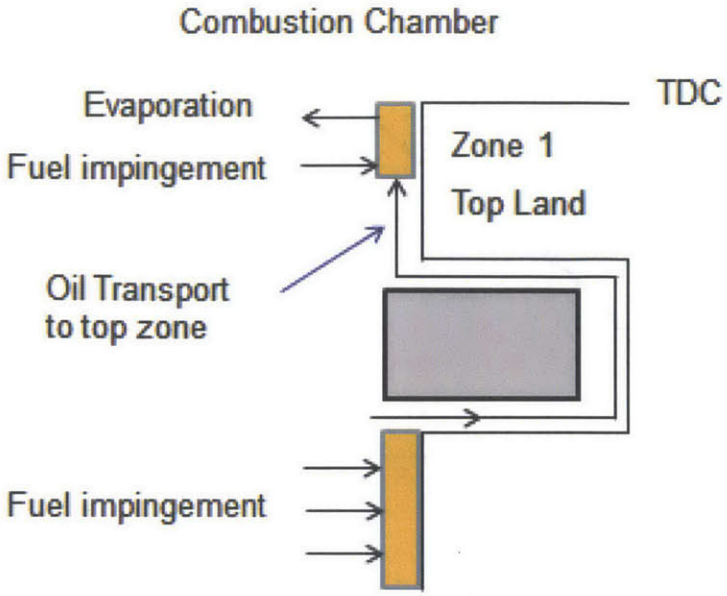

Figure 6-9: Schematic with fuel impingement along entire cylinder liner

spray geometries and the angle in which fuel is sprayed onto the cylinder liner can be further built upon in future studies for the composition model. For now, the fuel dilution rate of 5% is used to understand its general effects on oil viscosity.

Another modeling assumption is related to the fuel component species that retains in the oil and does not vaporize. All fuel composition components cannot be added because the lighter species will vaporize and only the heavier ones contribute to that 5%. To figure out which of the fuel species to include, an overlap of a biodiesel and diesel distillation curve is used. It is studied that most of the biodiesel components actually remain in the oil and assumed that components with those similar boiling point ranges will react in a similar manner for diesel. It is found that there is an overlap of 320°C-370°C boiling points for these two types and an average of 345°C is used. This corresponds well for a $C_{25}H_{52}$ species and this species viscosity components will be used when using the blending equation. Another method that can be used is to look at the distillation curve for diesel only and assume a percent of it to the left is vaporized and a percent of it on the right is not. This method even though it works will lead to roughly the same result as the first method.

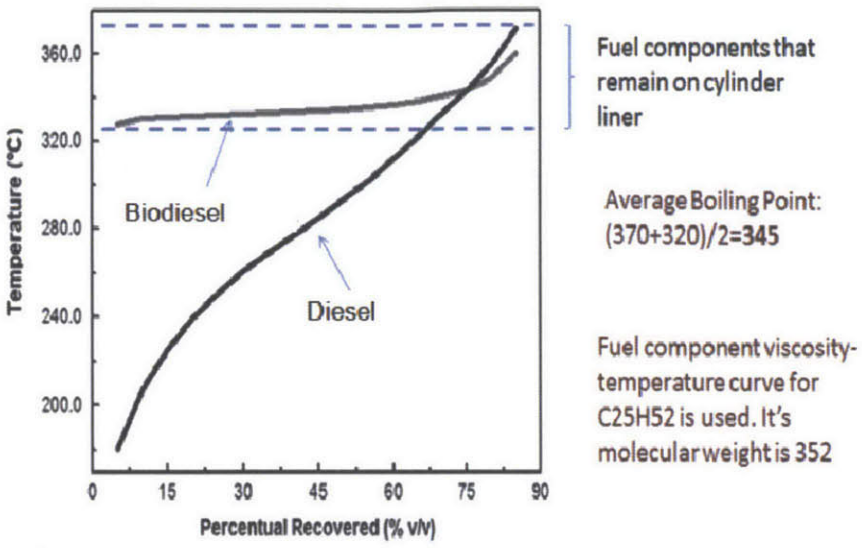

Figure 6-10: Diesel fuel components overlap with that of biodiesel at boiling points 320°C-370°C, with a boiling point of 345° on average

6.2.7 Fuel Dilution Results on Viscosity

Results from fuel impingement using the methodology above is shown in Figure 6-11. The three curves shown include temperature effects only, vaporization and temperature effects, and also fuel impingement effects with using a $C_{25}H_{52}$ hydrocarbon component fuel. Two of the curves are the same as ones mentioned in the previous chapter that included vaporization and temperature. The only additional curve is fuel impingement. The goal was to see the effects of fuel impingement on viscosity and it can be seen that the viscosity curve with vaporization is shifted down when considering fuel dilution effects. The viscosity at TDC decreased from 11 cST to 7 cST, which amounts to a 57% decrease.

Viscosity decreases are highly dependent on the fuel components that actually impinge on the oil and their individual component viscosity. Effects of using a lighter fuel such as $C_{14}H_{30}$ is also looked at and can be seen that there is a greater decrease in visosity as a result of using a lighter fuel component (Figure 6-12). This makes sense because with a lighter fuel component composition, the component viscosity is lower and there is a bigger effect on the overall mixture viscosity as can be seen

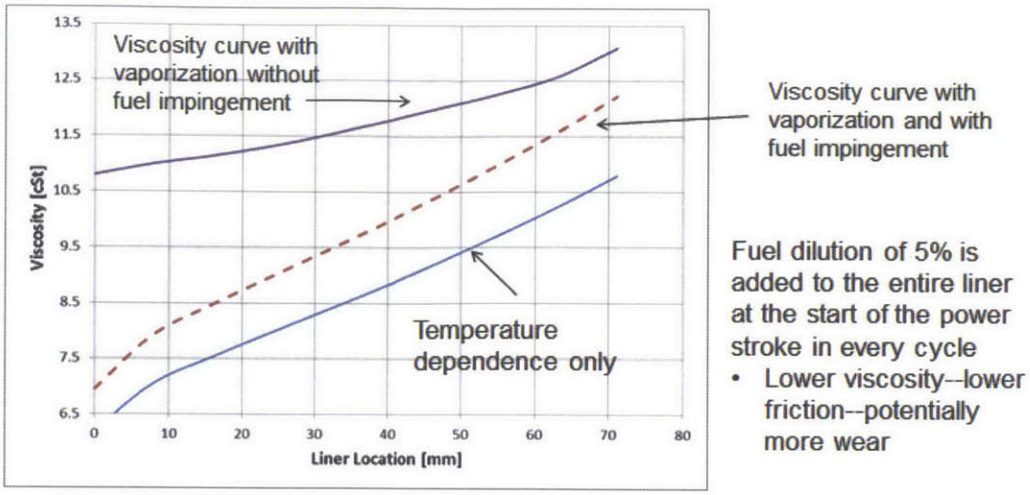

Figure 6-11: Viscosity results from fuel dilution shows a 57% decrease in viscosity near TDC.

from the blending equation. It can be noted that the effects of fuel dilution is very dependent on the fuel component that actually remains in the oil. If a lighter or heavier hydrocarbon is chosen, the results of the oil composition model would be vastly different. The assumptions for this study plays a big role in the actual results. Next the results of this study will be compared and validated through industry knowledge and experience.

6.2.8 Validation of Fuel Dilution Results

To determine whether the simulation results are in the correct magnitude, the group consulted industry. The industry sponsor explained that with 1% fuel dilution at 100°C shows about a 0.5 cST decrease in viscosity. This involves using 1% fuel dilution in the simulation results to do a comparison (Figure 6-13). Looking at the location of 50 mm which corresponds to about 100°C in liner temperature, there is a fuel dilution of about 0.3 cST (12.2-11.9). 0.3 cST is relatively close to the drop of 0.5 cST mentioned by industry experience, meaning there is a relatively good correspondence.

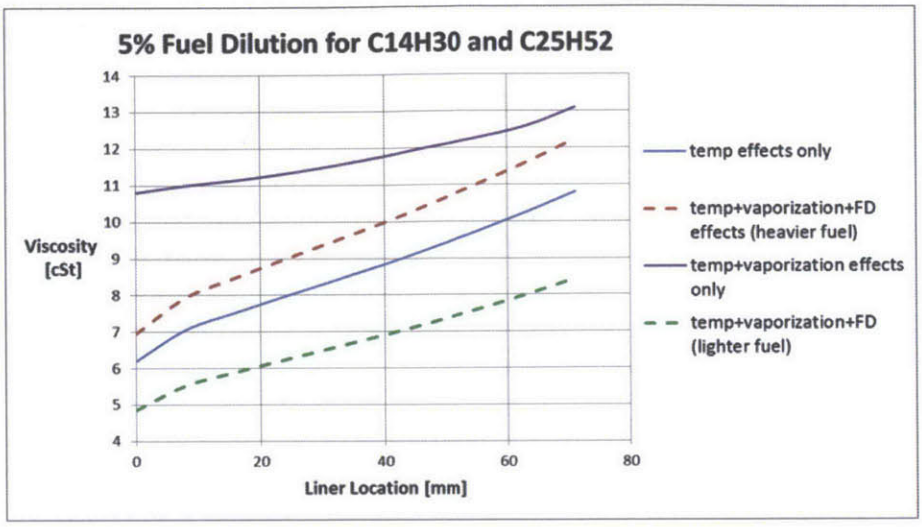

Figure 6-12: The addition of lighter fuel fractions causes a bigger drop in viscosity due to fuel dilution

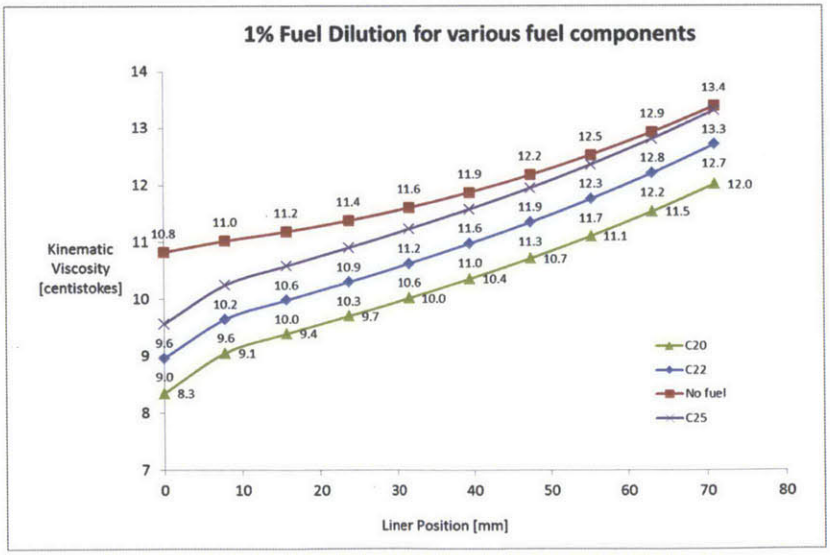

Figure 6-13: Simulation results show a good match with industry knowledge

6.3 Soot Contamination

Of the many contaminants in the engine, fuel dilution and soot are two prevalent ones. This section will discuss soot contamination and its effects on viscosity through compositional modeling. The section includes an introduction to soot oxidation and formation, soot in oil viscosity approximations using Einstein's Equation, and also oil oxidation effects included in engine tests.

6.3.1 Introduction

A lot of emphasis is put on the downstream effects of soot and how to optimize the individual components of DPF to get rid of as much soot is produced as possible. This device has proved to be effective in getting rid of an astonishing 99% or more of the soot that exits the exhaust. However, it is noteworthy that most of the soot formed in the cylinder is oxidized in cylinder before going out to the exhaust and into the filter. Roughly 90% of the soot formed is oxidized and therefore less than 10% of the soot formed exits the combustion chamber. That means that the DPF's goal is to get rid of the 10% of the soot actually formed. All this focus on optimizing the after-treatment system for 10% of the soot would not be as efficient as thinking upstream and focusing on what happens in the cylinder where all the soot is actually formed and oxidized. This section's motivation will focus on upstream effects, where soot is actually created in the cylinder.

6.3.2 Soot Formation

Soot particles form from the carbon in the diesel fuel. The formation process starts with a fuel molecule containing 12 to 22 carbon atoms and an hydrogen to carbon ratio of about 2. The process ends up with particles typically a few hundred nanometers in diameter, composed of spherules 20 to 30 nanometers in diameter each containing some 10^5 carbon atoms and having an hydrogen to carbon ratio of 0.1.

Soot formation takes place in the diesel combustion environment at temperatures between about 1000 K and 2800 K, at pressures of 50 to 100 atm, and with sufficient

Figure 6-14: Contaminated soot oil on very right compared with clean oil on left

air overall to burn full all the fuel. The time available for the formation of solid soot particles from a fraction of the fuel is in the order of milliseconds. The soot formation process consists of two stages: particle formation and particle growth. Particle growth includes both surface growth, coagulation, and aggregation.

At each of these stages,oxidation can occur where soot is burned in the presence of oxidizing species to form gaseous products such as CO and CO_2 which will be described in more detail in the next subsection. The eventual emission of soot from the engine will depend on the balance between these processes of formation and burnout [23].

6.3.3 Soot Oxidation

High temperature combustion takes place inherently in flames after the formation of soot. For instance, it is estimated that more than 90 % of the soot formed in diesel engines is combusted before the exhaust gases leave the cylinder. Once soot nucleation has occurred, the amount of soot generated is determined by the competing processes of growth through the addition of gas phase species and destruction through oxidation species. There are many species in or near the flame that could oxidize soot and examples include O_2, O, OH, CO_2, H_2O. and NO_2. These species attach to soot carbon particles and convert them to less harmful gaseous species [23].

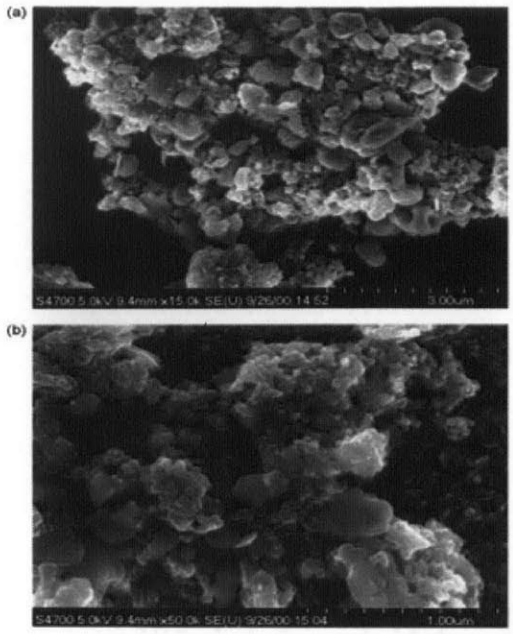

Figure 6-15: SEM images of soot particles in oil [1]

6.3.4 Soot Contaminated Oil

During the combustion process, soot particles are produced and are either exhausted into the atmosphere or absorbed by the engines lubricant(Figure 6-15). Soot reaches the engine oil by blowby gases that combine with antiwear and viscosity additives in the oil and also reaches the engine oil on the cylinder walls. Figure 6-14 shows the difference between good uncontaminated oil with soot contaminated oil. The photo on left is fresh clean oil before putting it into the engine. The oil in the middle is oil sampling from the valvetrain when using a split system in which the valvetrain sump is separate from the power cylinder sump. The oil on right is oil sampling from power cylinder. This is only after 6 hours of running time. This experiment was done to see if there is any difference in degradation of oil when using a split system. The piston ring pack experiences harsh operating conditions and processes such as vaporization and fuel impingement. The valve-train on the other hand does not experience the harsh conditions like the power cylinder. Using the split system idea can help researchers tailor lubricant formulations to valve-train conditions and create a longer lasting valve-train oil specific to valve-train. As can be seen in the

valve-train sampled oil, it looks similar in color as the new oil. The power cylinder oil on the other hand is completely black and contaminated from soot. The impact of soot in the oil can be seen clearly here and is clearly a concern when considering engine oil quality.

6.3.5 Dispersants

The main reason for adding dispersants to diesel engine oils has been due to the increasing levels of soot. The level of soot in diesel engine oil has trended higher as a result of new engine technologies designed to reduce NO_X and particulate emissions. Retarded fuel injection has been one of the main strategies employed by OEM's to reduce NO_X emissions, which resulted in more unburned fuel entering the crankcase oil as soot particles. Dispersants have a polar head group with an oil-soluble hydrocarbon tail and its main function is to minimize the deleterious effects of soot contaminants (Figure 6-16). In modern top-quality engine oil formulations, dispersants range from 3 to 6% by weight.

Soot particles are attracted to one another by Van Der Waals forces and agglomerates to form larger particles when they collide. These particles which start out as 20 nanometers in diameter can become 2 micrometers in diameters when they agglomerate. The job of the dispersant additive is to keep the soot particles finely divided and off of machine surfaces. It disperses these contaminants within the engine thereby ensuring that the oil flows freely.

The additive works by enveloping the soot particle. The polar head of the dispersant molecule clings to the particle directing the additives "oleophillic" tail outward to dissolve easily into the oil, prohibiting particle from agglomerating with other soot particles or depositing onto component surfaces. Dispersants provides once-through protection. Once it is depleted, dispersancy is lost, leaving the machine at risk. Soot uses up dispersants and once all the dispersants are used, there will not be any more left and then the soot will start agglomerating at great lengths and getting on the surface which is a danger to the engine oil [18].

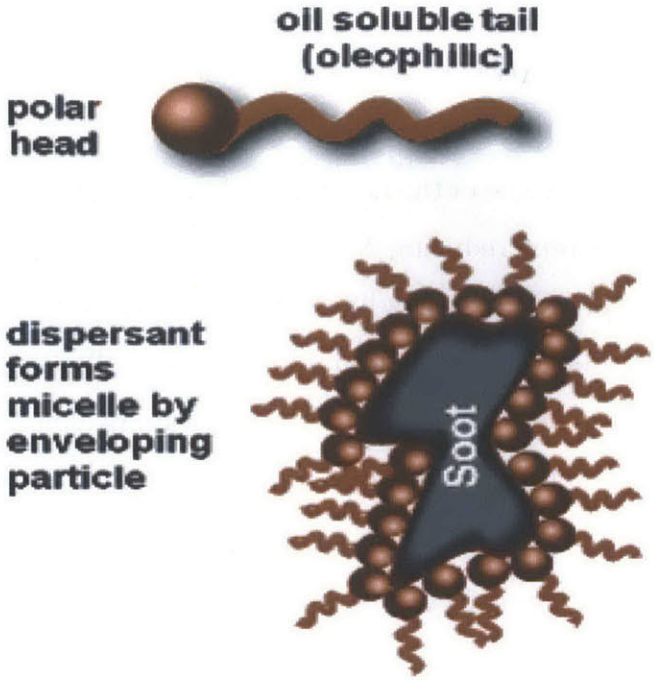

Figure 6-16: Dispersants have a polar head with an oil-soluble hydrocarbon tail [22]

6.3.6 Effects of Exhaust Gas Recirculation

Exhaust gas recirculation (EGR) is one of the effective means to reduce the NO_X emission from diesel engines. Tier 4 requirements for NO_X (Table 6.1) shows that NO_X emissions in grams depends on how long you run the engine for and what is the rated power. Running an engine for 6 hours at rated power of 100 Kilowatts allows for 20.4 grams of NO_X emissions.

EGR process returns exhaust product to the diesel engine combustion chamber

Pollutant [g/KWh]	Engine Rated Power [KW]		
	< 56	56-129	130-560
NOX	——	3.4	2
PM	0.03	0.02	0.02
CO	5	5	3.5

Table 6.1: Interim Tier 4 Criteria Pollutant Limits

and accelerates the degradation of the lubricant engine oil, primarily by increasing the total acid number (TAN) as well as the soot content and, consequently, the viscosity. EGR involves recirculation of exhaust gas back into the intake stream. The recirculated gas displaces some of the normal intake charge, which slows and cools the combustion process, thereby reducing NOX formation. The use of EGR will increase the soot and other solid paniculate loading of the lubricant oil. Re-introduction of the acidic exhaust gas product (sulfuric acid) into the engine will rapidly increase the total acid number (TAN) of the lubricant. Accelerated rate of lubricant oil degradation will lead to relatively short oil drain intervals [1].

6.3.7 Soot and Viscosity Changes

Soot contamination of the lubricating oil causes viscosity of the lubricant to increase and also pumpability problems that induces wear. An increase in viscosity depends on the percent of soot in the oil drain, particle size of soot, and surface area of soot dispersed in the oil [8]. Figure 6-17 shows viscosity curves at two different temperatures. The empirical data equations are also shown on the curves [7]. Viscosity curves and effects of soot contamination varies for different temperature ranges. There is a greater viscosity increase as soot percentage is increased.

6.3.8 Soot Modeling and Assumptions

To model soot, some assumptions can be made to make approximations:

- 90 % of soot formed is oxidized prior to exhaust
- 1 % of soot to exhaust gets absorbed into liner
- Soot populates zones closest to the flame
- The diameter of a soot particle is around 20nm
- The density of soot is 2 g/cm^3
- Dispersants are capable of keeping soot disperased in solution and not agglomerating

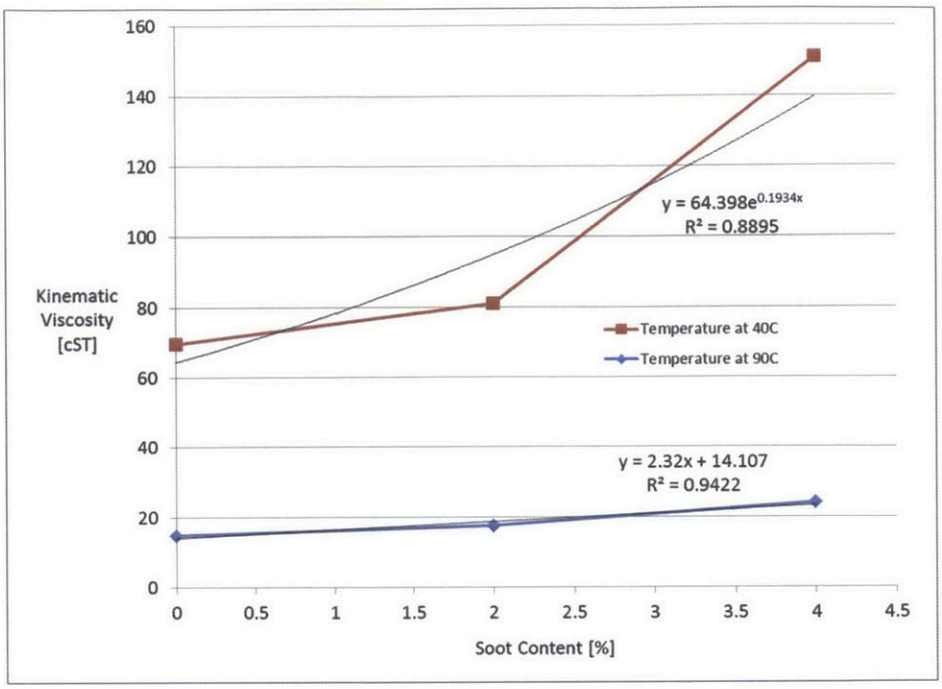

Figure 6-17: Kinematic Viscosity of oil samples at 40 and 90 degrees C at the different soot levels

The soot distribution is assumed to be increasing as we move up toward the liner zones. For example, there would be more soot particles in the first zone of the cylinder liner oil than the second zone and so forth (Figure 6-18).

The goal is to obtain how much soot is created per cycle of engine running time to see how much soot to add to the model. To obtain this, detailed analysis of this number is to be calculated and can be determined in future refining of the soot contamination component of the model. The thesis goal is to set up for the modeling of the soot particles and look at approximate effects on viscosity. The next subsection discusses one method of determining this value.

6.3.9 Soot Balance

The general equation for soot balance is shown below:

$$soot_{formed} = soot_{oil} + soot_{oil-filter} + soot_{exahust} + soot_{oxidized} \tag{6.1}$$

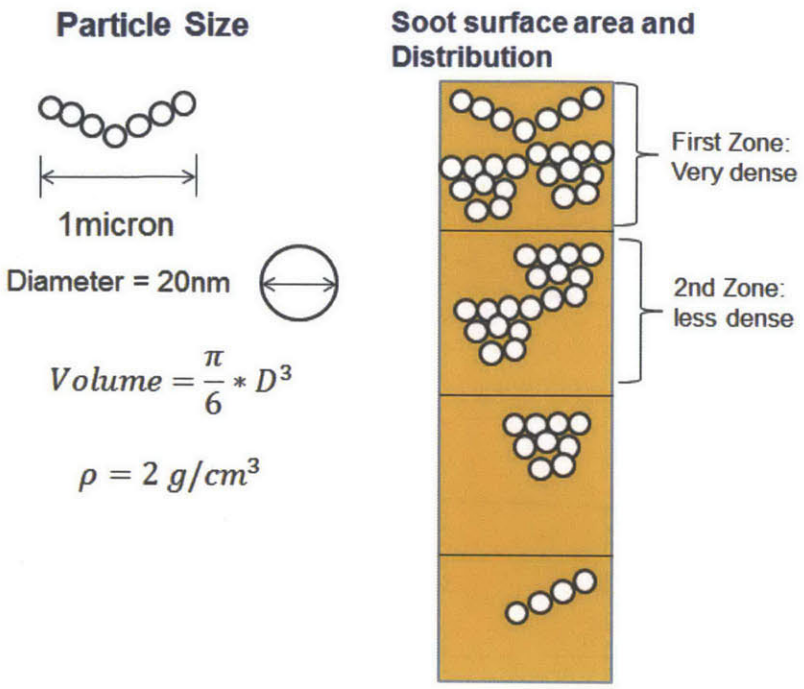

Figure 6-18: Assumptions for soot modeling

where $soot_{formed}$ is the amount of soot formed in the engine during a cycle, $soot_{oil}$ is the amount of soot that actually gets into the engine oil and contaminates it, $soot_{oil-filter}$ is the amount of soot that the oil filter is able to filter out, $soot_{exahust}$ is the amount of soot that actually goes out of the engine exhaust into the aftertreatment systems, and finally $soot_{oxidized}$ is the amount of soot that is oxidized by other species in the engine. Using a soot balance could be one method to obtain the amount of soot in the oil at every given cycle. Other methods could include using a mass transfer approach to calculate how much of the soot lands on the oil on the liner and how much remains in the gaseous phase. Understanding the probability of soot sticking to the liner is a complicated task and can be further studied in a future soot modeling.

6.3.10 Empirical Data

To get a general idea of how much increase in viscosity is from soot contamination, empirical data was studied. There are a lot of research papers discussing experiments done with soot contaminated oil and how does the viscosity change. One such example

Table 1
Some properties of new and used oils from M-1 1 engine test

	A (new oil)	B	C
Viscosity at 100 °C (cSt) (start of engine test)	14.40	14.39	14.55
Viscosity at 100 °C (cSt) (end of engine test)	-	24.95	42.91
Total acid number (TAN)	1.1	3.81	2.08
Total base number (TBN)	10.43	8.42	6.11
Soot content (%)	0	6.9	9.0

Figure 6-19: Engine data shows an increase from 14 cST viscosity to 42 cST viscosity for 9% soot content [1]

is Figure 6-19 shows for different soot content percentage, the change in viscosity from the baseline viscosity at the start of the engine test around 14 cST [1].

However, what is important to note is that these are engine tests and the tests did not isolate soot effects from other effects. Another big contamination effect is oil oxidation. The method to incorporate oil oxidation effects are discussed below.

6.3.11 Oil Oxidation

Oil oxidation occurs when oxygen molecules chemically join with oil molecules. Oxidation is accelerated by high oil temperature and causes the oil to thicken, form acids, and lose lubrication qualities. Oil oxidation effects on viscosity is extremely difficult to model due to the differences of oxidation rates for different types of oil. As a result, oil oxidation is not modeled in this current composition model. To examine the coupled effects of oil oxidation, Sequence IIIG engine tests were investigated [6]. The procedure explains that viscosity increase due to oxidation cannot exceed 150%. This can be applied to the oil composition model as the maximum limit that oil oxidation can affect oil viscosity.

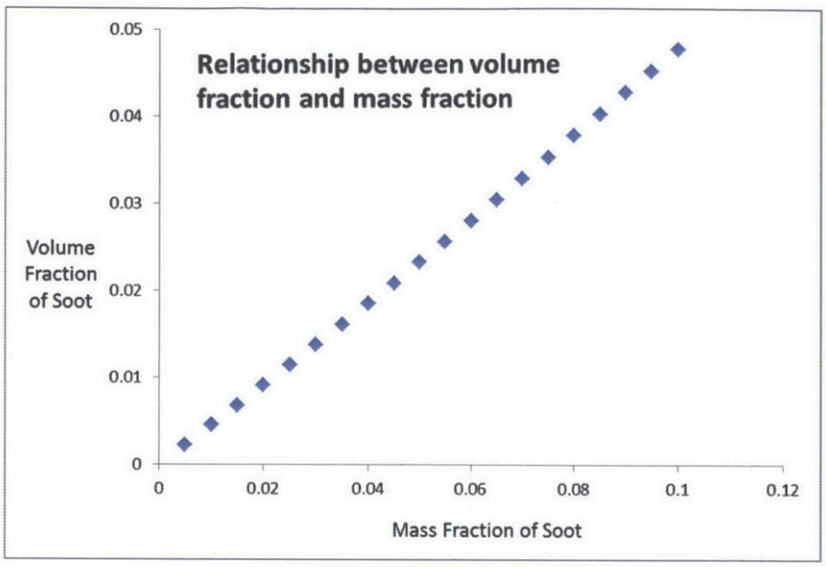

Figure 6-20: 10% mass fraction of soot corresponds to a volume fraction of 0.05

6.3.12 Einstein Equation Approximation

Engine data includes many of the contamination sources such as oxidation discussed above and soot contamination. Soot particles are approximated as spherical shaped with a diameter around 20 nanometers. To observe the effects of spherical particles in a dilute oil solution, Einstein's equation can be used and shown below [12]

$$\nu_{soot} = \nu(1 + 2.5 * \phi) \tag{6.2}$$

where ν_{soot} is the effective viscosity of a dilute suspension of soot, ν is the viscosity of the ambient fluid without spheres, and ϕ is the volume fraction of spheres in suspension. Einstein's equation can be used only for a dilute suspension of spherical particles. Mentioned above, dispersants are the additive in the oil that keep soot from agglomerating and in suspension. Using this equation, it is assumed that dispersants are doing their job and not completely depleted so that Einsteins equation holds that there is no agglomeration occurring and the particles are suspended.

Making a rough estimation of how much increase in viscosity there would be for the suspension of soot spherical particles, one can assume that there is roughly 10% mass fraction of soot at the end of each oil drain interval, which is consistent with

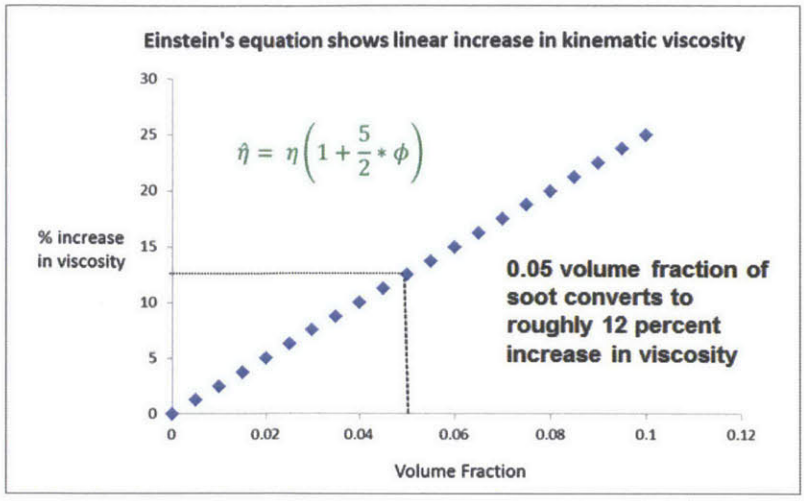

Figure 6-21: 0.05 volume fraction of soot corresponds to a 12% increase in viscosity according to Einstein's Equation.

literature engine data within a few percent. A 10% mass fraction of soot corresponds to a 0.05 volume fraction, using a density of oil as 900 kg/m^3, and density of soot as 2000 kg/m^3 (Figure 6-20).

Using a volume fraction of 0.05 and plugging it into the Einstein's Equation to observe its effects on viscosity shows a 12% increase in visosity due to these spherical particles (Figure 6-21). Looking at empirical data in the previous section, there is clearly a greater than 12% increase in viscosity. The reason for this is due to the oil oxidation effects that thicken oil. Taking oil oxidation 150% increase in viscosity and an additional 12% from Einstein's Equation, gives a total of 180% increase in viscosity (1.12*2.50). Looking at the engine test data for 9% soot (Figure 6-19), there is a viscosity increase of (42.91 cSt-14.55 cSt)/14.55 cSt which corresponds to 195% increase in viscosity.

The differences between the theoretical estimate and experimental values of 180 and 195% increase in viscosity could be due to many things. It shows that there are many more phenomenons going on and is not captured solely through soot contamination and oil oxidation. Other processes that could be taken account are oil volatility and gas absorption onto the liner, changing its TBN and TAN. The processes are indeed very complex and can be considered in future work.

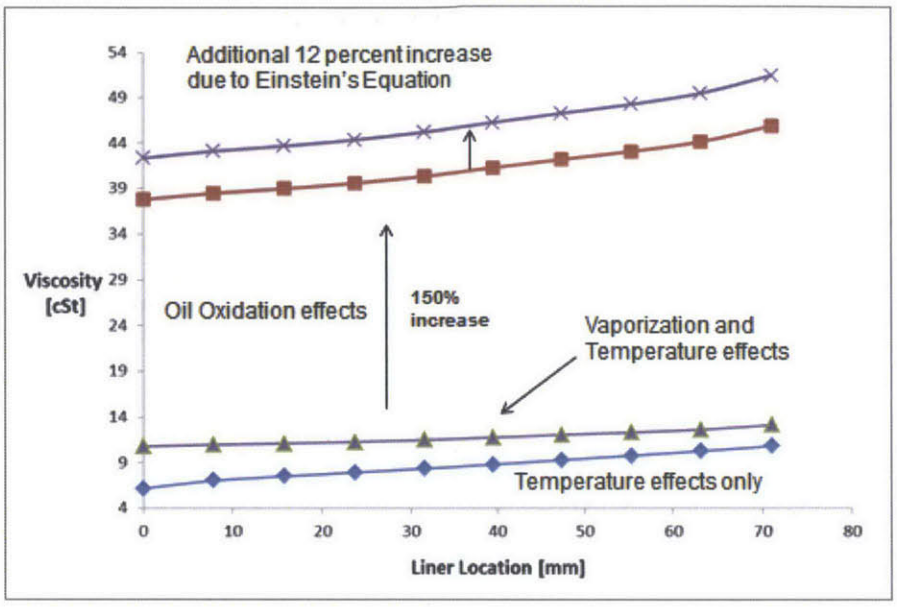

Figure 6-22: Combined effects of oxidation and soot contamination shows an additional 180% increase in viscosity.

6.3.13 Combined Effects of Soot and Oil Oxidation

The combined effects of oil oxidation and soot along with vaporization and temperature effects are shown in Figure 6-22. The figure shows the original temperature and vaporization effects curve that was portrayed in the previous chapter of rheology. The addition of oxidation raises the viscosity by 150% and the addition of soot spherical particles raises the viscosity by an additional 12%. This shows the significance of understanding the processes going on to see the changes in viscosity it can cause.

Chapter 7

Conclusions

This final chapter summarizes the different concepts discussed in this thesis and also discusses future work that can be conducted.

7.1 Summary

The motivation behind an oil composition model was discussed in the introduction and involves the ability to optimize lubricant formulations for higher fuel efficiency. Viscosity changes due to many processes such as degradation, vaporization, and soot contamination. Lubricant formulation can be designed to resist changes in viscosity through high quality base oils, antioxidants, and viscosity modifiers. Oil Composition is one of the drivers that affect viscosity and therefore be used as a lever to improve fuel economy of the engine.

Past literature on oil composition modeling was discussed. Audette, Cho, and Liang did thorough research on Vaporization. However, they did not combine composition with viscosity, which is the basis of this work. In addition, their work did not go beyond vaporization, whereas this thesis work extends to many other applications and processes.

The first physical process discussed is oil mixing due to piston movement. Axial mixing analysis shows that mixing only occurs when the piston ring is above the oil particle location. Flow rates are calculated at each liner position from using piston

speed, film thickness, and pressure gradient parameters. From this basic model of oil transport, chemical processes are applied to each species in each different liner location. The species used in this study includes a combination of 13 different paraffin species that make up a typical 15W40 SAE oil.

For the process of vaporization, due to high temperatures near the top dead center of the piston, light volatile hydrocarbons vaporize and leave the system. Light carbon number species disappear at a faster rate due to their high volatility and vaporization rates. This results in retention of heavier hydrocarbon species near the top zone of the cylinder liner model. Vaporization rates for different species in each liner location are obtained by looking at individual vapor pressures, mass transfer coefficients, and other oil properties.

Composition changes due to vaporization were solved for and the link between composition and viscosity is a blending equation. The Arrhenius blending equation is used to calculate mixture viscosity from the summation of different species composition and component viscosity values. A combination of composition results obtained from the above analysis and blending equations for mixtures shows that near the top dead center or top zone, the viscosity is higher than just considering temperature effects on oil viscosity. The impact of this vaporization component shows that the addition of a non-volatile oil species near the top dead center of the cylinder liner has the ability to flatten the species viscosity versus liner location curve.

Late injections of fuel can result in impingement of liquid fuel on the surfaces of the combustion chamber. Typical design for fuel in oil limit dilution is 5% so for modeling purposes, it is assumed that there is a 5 percent fuel dilution rate and this addition of fuel is added during each power stroke of the engine cycle. Heavier parts of fuel are used in this analysis because lighter parts of fuel will vaporize and not stay in the engine oil and contaminating it. Compositional changes due to fuel dilution and vaporization was calculated and then used in the Arrhenius blending equation to solve for new mixture viscosity. Results from fuel shows that the viscosity curve is shifted downwards when considering fuel dilution effects. This corresponds well with experimental data because experiments also show a decrease in viscosity due to

fuel dilution because of fuels lower viscosity compared with engine oil. This decrease in viscosity shows that fuel dilution has the detrimental ability to reduce the oil lubricating properties and actually lead to increased wear in the engine.

Other applications such as additive concentration and soot contamination are discussed. For additive concentration, enrichment factors were calculated from the oil composition model and shown to be in the same magnitude as experimental data for enrichment factors in another study at MIT [25], showing a good correlation between experiment and simulation. Soot contamination causes a change in viscosity of oil due to soot particles getting into the lubricant. To calculate how much of a change of viscosity there is, Einstein's equation was applied. To compare with experimental engine tests, oil oxidation effects needed to be taken account. Oil oxidation, due to its difficulty in modeling it, is taken to increase viscosity of oil 150 % as a maximum value according to Sequence III engine tests. Oil oxidation and Einstein's equation of sphere particles are both taken account when determining soot contamination effects to validate with engine tests.

This new oil composition model solves for in situ-compositional changes for different oil species due to different physical and chemical processes along the cylinder liner. This change in composition causes a change in viscosity of the overall mixture which is solved for with blending equations. Then from mixture viscosity values, friction and wear can then be calculated to optimize the lubricant for fuel efficiency.

7.2 Future Work

A lot of physical and chemical processes can occur on the cylinder liner oil. Other applications that were not discussed in detail but of which should definitely needed to model are: oil oxidation, combustion gas contamination, and scraping oil transport mechanism.

For the current processes, oil scraping can be explained in the oil transport portion. Dragging was the main focus of this work, but oil scraping can also have a major effect on oil composition along the liner. Fuel dilution effects can also be studied in more

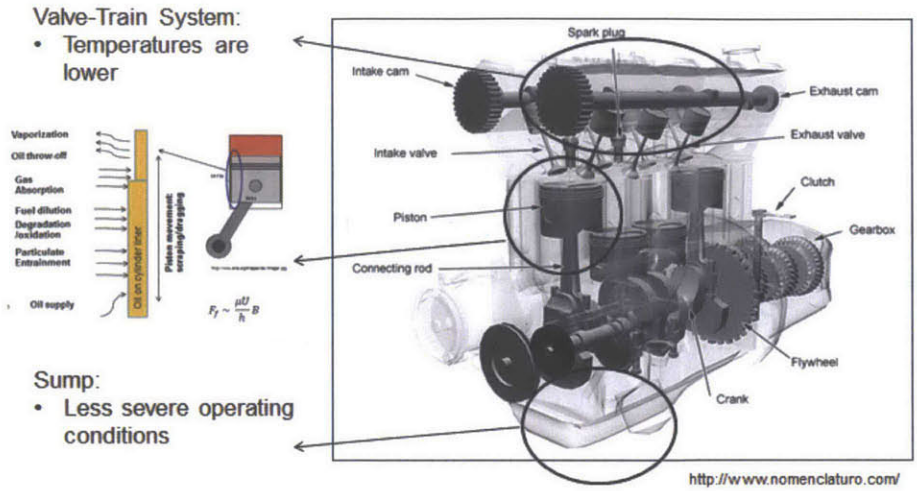

Figure 7-1: Future applications of oil composition can expand to other zones in the engine

detail by not assuming a 5% fuel dilution percentage and actually solving for the amount of fuel dilution considering the injector dimensions and geometry and spray angles. Soot contamination was only approximated in this thesis, but can be studied in more detail as to how soot actually gets into the oil and what is the probability of soot sticking to the oil rather than staying in the gas phase.

These major chemical processes occur mainly in the ring pack zone, which was the focus of the study due to the majority of mechanical friction occurring between the piston rings and cylinder liner region. However, there are other interactions from different zones. The sump, valve-train, and crankshaft main bearings oil all communicate with each other. The valve-train composition is vastly different from the ring pack zone's and this difference can be studied in the future. This shows that an oil composition model, given different inputs, can be used for many different applications.

Bibliography

[1] S. Aldajah, O. O. Ajayi, G. R. Fenske, and I. L. Goldblatt. Effect of exhaust gas recirculation (EGR) contamination of diesel engine oil on wear. *Wear*, 263(16):93–98, September 2007.

[2] Morgan Andreae, Howard Fang, and Kirtan Bhandary. Biodiesel and fuel dilution of engine oil. SAE Technical Paper 2007-01-4036, SAE International, Warrendale, PA, October 2007.

[3] William E. Audette. *Estimation of oil consumption due to in-cylinder vaproization in internal combustion engines.* PhD thesis, Massachusetts Institute of Technology, 1999.

[4] Haijie Chen. *Modeling the lubrication of the piston ring pack in internal combustion engines using the deterministic method.* Thesis, Massachusetts Institute of Technology, 2011. Thesis (Ph. D.)–Massachusetts Institute of Technology, Dept. of Mechanical Engineering, 2011.

[5] Yeunwoo Cho. *Modeling engine oil vaporization and transport of the oil vapor in the piston ring pack on internal combustion engines.* PhD thesis, Massachusetts Institute of Technology, 2004.

[6] D02 Committee. Test method for evaluation of automotive engine oils in the sequence IIIG, spark-ignition engine. Technical report, ASTM International, 2013.

[7] Sam George, Santhosh Balla, and Mridul Gautam. Effect of diesel soot contaminated oil on engine wear. *Wear*, 262(910):1113–1122, April 2007.

[8] Sam George, Santhosh Balla, Vishaal Gautam, and Mridul Gautam. Effect of diesel soot on lubricant oil viscosity. *Tribology International*, 40(5):809–818, May 2007.

[9] J. A. Greenwood and J. H. Tripp. The contact of two nominally flat rough surfaces. *Proceedings of the Institution of Mechanical Engineers*, 185(1):625–633, June 1970.

[10] John B. Heywood. *Internal combustion engine fundamentals.* McGraw-Hill, 1988.

[11] Kenneth Holmberg, Peter Andersson, and Ali Erdemir. Global energy consumption due to friction in passenger cars. *Tribology International*, 47:221–234, March 2012.

[12] Arkady L. Kholodenko and Jack F. Douglas. Generalized stokes-einstein equation for spherical particle suspensions. *Physical Review E*, 51(2):1081–1090, February 1995.

[13] Hans Korsten. Viscosity of liquid hydrocarbons and their mixtures. *AIChE journal*, 47(2):453462, 2001.

[14] Liang Liu. *Modeling the performance of the piston ring-pack with consideration of non-axisymmetric characteristics of the power cylinder system in internal combustion engines.* PhD thesis, Massachusetts Institute of Technology, 2005.

[15] Michael L. McMillan, Edward P. Becker, and Shirley E. Schwartz. Handbook of lubrication and tribologysimon c. tung and. 2006.

[16] Michael J. Plumley, Victor Wong, Mark Molewyk, and Soo-Youl Park. Optimizing base oil viscosity temperature dependence for power cylinder friction reduction. Technical Report 2014-01-1658, SAE International, Warrendale, PA, April 2014.

[17] Robert C. Reid. Handbook on vapor pressure and heats of vaporization of hydrocarbons and related compounds, r. c. wilhort and b. j. zwolinski, texas A&M research foundation. college station, texas (1971). 329 pages. $10.00. *AIChE Journal*, 18(6):1278–1278, November 1972.

[18] Leslie R Rudnick. *Lubricant additives chemistry and applications.* CRC Press, Boca Raton, FL, 2009.

[19] Christopher J. Seeton. Viscositytemperature correlation for liquids. *Tribology Letters*, 22(1):67–78, April 2006.

[20] Robert Sutton and David Bergman. Application of the bergman-sutton method for determining blend viscosity. Society of Petroleum Engineers, October 2008.

[21] Tian Tian. *Modeling the performance of the piston ring-pack in internal combustion engines.* Thesis, Massachusetts Institute of Technology, 1997. Thesis (Ph. D.)–Massachusetts Institute of Technology, Dept. of Mechanical Engineering, 1997.

[22] Drew Troyer. Get ready for more soot in engine oil. *Machinery Lubrication*, 1999.

[23] Barry A. A. L. van Setten, Michiel Makkee, and Jacob A. Moulijn. Science and technology of catalytic diesel particulate filters. *Catalysis Reviews*, 43(4):489–564, 2001.

[24] Syed Wahiduzzaman, Rifat Keribar, Zafer Dursunkaya, and Frank A. Kelley. A model for evaporative consumption of lubricating oil in reciprocating engines. SAE Technical Paper 922202, SAE International, Warrendale, PA, October 1992.

[25] Simon A. G. (Simon Andrew Glean) Watson. *Lubricant-derived ash : in-engine sources and opportunities for reduction.* Thesis, Massachusetts Institute of Technology, 2010. Thesis (Ph. D.)–Massachusetts Institute of Technology, Dept. of Mechanical Engineering, 2010.

[26] Ertan Yilmaz. *Sources and characteristics of oil consumption in a spark-ignition engine.* Thesis, Massachusetts Institute of Technology, 2003. Thesis (Ph. D.)–Massachusetts Institute of Technology, Dept. of Mechanical Engineering, 2003.

[27] Rob Zdrodowski, Arup Gangopadhyay, James E. Anderson, William C. Ruona, Dairene Uy, and Steven J. Simko. Effect of biodiesel (b20) on vehicle-aged engine oil properties. SAE Technical Paper 2010-01-2103, SAE International, Warrendale, PA, October 2010.